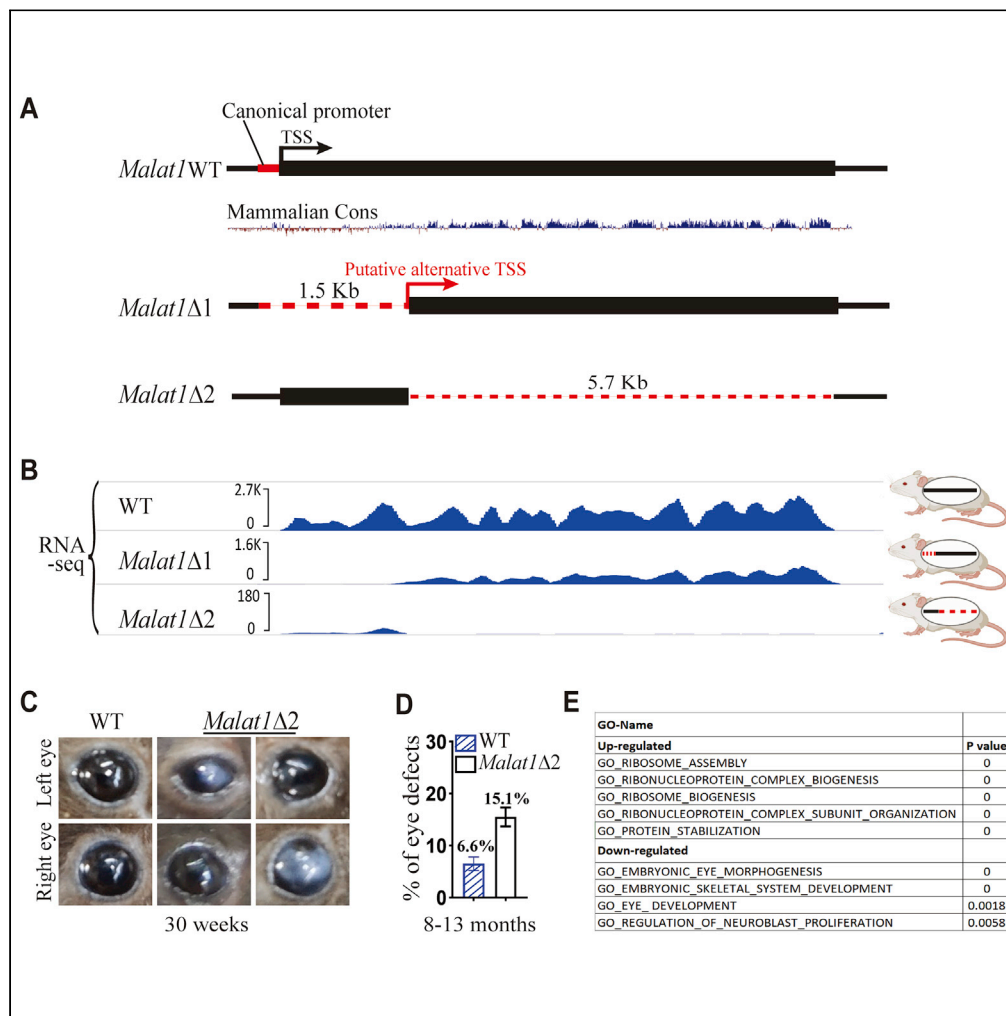## Article

Alternative transcribed 3′ isoform of long non-coding RNA *Malat1* inhibits mouse retinal oxidative stress

Amr. R. Ghanam, Shengwei Ke, Shujuan Wang, ..., Tian Xue, Yong Zheng, Xiaoyuan Song

zy@ncpsb.org.cn (Y.Z.)
songxy5@ustc.edu.cn (X.S.)

Highlights

Malat1 is upregulated in replicative senescence (*in vitro*) and brain aging (*in vivo*).

A potential cryptic promoter drives 3′*Malat1* isoform expression in mouse brain & retina

Deletion of the 3′-*Malat1* isoform region increases retinal oxidative stress in mice

5′& 3′*Malat1* transcripts differentially regulates gene expression *in cis* & *in trans*

iScience

Article

Alternative transcribed 3′ isoform of long non-coding RNA *Malat1* inhibits mouse retinal oxidative stress

Amr. R. Ghanam,[1,6] Shengwei Ke,[1,3,6] Shujuan Wang,[2] Ramy Elgendy,[4] Chenyao Xie,[1] Siqi Wang,[1] Ran Zhang,[1] Min Wei,[1] Weiguang Liu,[1] Jun Cao,[1] Yan Zhang,[5] Zhi Zhang,[1] Tian Xue,[1] Yong Zheng,[2,*] and Xiaoyuan Song[1,7,*]

SUMMARY

The function of the cancer-associated lncRNA *Malat1* during aging is as-of-yet uncharacterized. Here, we show that *Malat1* interacts with Nucleophosmin (NPM) in young mouse brain, and with Lamin A/C, hnRNP C, and KAP1 with age. RNA-seq and RT-qPCR reveal a persistent expression of *Malat1_2* (the 3′isoform of *Malat1*) in *Malat1Δ1* (5′-1.5 kb deletion) mouse retinas and brains at 1/4th level of the full-length *Malat1*, while *Malat1_1* (the 5′isoform) in *Malat1Δ2* (deletion of 3′-conserved 5.7 kb) at a much lower level, suggesting an internal promoter driving the 3′ isoform. The 1774 and 496 differentially expressed genes in *Malat1Δ2* and *Malat1Δ1* brains, respectively, suggest the 3′ isoform regulates gene expression *in trans* and the 5′ isoform *in cis*. Consistently, *Malat1Δ2* mice show increased age-dependent retinal oxidative stress and corneal opacity, while *Malat1Δ1* mice show no obvious phenotype. Collectively, this study reveals a physiological function of the lncRNA *Malat1* 3′-isoform during the aging process.

INTRODUCTION

Long non-coding RNAs (lncRNAs), or RNAs >200 nt, which remain untranslated although sometimes generate short peptides,[1] are estimated to pervasively transcribe from over 90% of the mammalian genome,[2,3] yet their physiological functions and underlying mechanisms are largely undefined.[4,5] In particular, lncRNAs are highly abundant in the brain, in terms of both diversity and copy number.[6,7] This is noteworthy since the brain is highly susceptible to aging.[8] However, the biological significance and underlying molecular mechanisms of the majority of brain-associated lncRNAs remain uncharacterized.[9]

The nuclear lncRNA *Malat1* (metastasis-associated lung adenocarcinoma transcript 1) is highly abundant in many tissues.[10,11] The 3′ end of *Malat1* can be processed into a 61 nt-RNA designated as *Malat1*-associated small cytoplasmic RNA (mascRNA); both the originating lncRNA and the processed mascRNA are highly conserved and widely distributed across a range of species, including *Danio rerio*, *Xenopus tropicalis*, *Mus musculus*, and *Homo sapiens*.

Emerging reports suggest that *Malat1* is a transcriptional regulator of gene expression,[12] and the *Malat1* locus is adjacent to another highly expressed nuclear lncRNA, *Neat1*, suggesting a shared pathway or complementary action for these two lncRNAs.[13] However, 5′ *Malat1* knockout (KO) mice, carrying a 3 kb deletion at the 5′ end of *Malat1* (consisting of regions 1.5 kb upstream and 1.5 kb downstream of the transcriptional start site, TSS), showed no phenotypic differences compared with wild-type (WT) mice[14] at an early age. Moreover, genetic ablation of *Malat1* by poly-A signal insertion at a position immediately downstream of TSS showed no effects on global gene expression, nuclear speckles, splicing factors, or alternative pre-mRNA splicing in mouse tissues, again at early age of examination.[15] Even the whole-length deletion of *Malat1* in mice leads to no obvious phenotype or histological abnormalities up to 6 weeks of age.[16] Despite its somewhat cryptic biological function, the evolutionary conservation of the *Malat1* 3′ region implies a potentially important biological role for this lncRNA.[17] Indeed, the essential function of *Malat1* in retinal neurodegeneration has been demonstrated, as researchers have found that *Malat1* is upregulated in retinas, Müller cells, and primary retinal ganglion cells (RGCs) under stress, where it interacts with cyclic AMP response element-binding protein to maintain its phosphorylation and promote survival in Müller cells and RGCs.[17] Likewise, knockdown of *Malat1* in cultured hippocampal

neurons, where it is abundantly expressed, decreases synaptic density while its overexpression results in a cell-autonomous increase in synaptogenesis, revealing the potential biological role of *Malat1* in synaptic plasticity.[18]

In the current study, we showed that in mice, *Malat1* is upregulated with age in the brain and especially in the retina. Through targeted deletion of a 5′-1.5 kb fragment (including the predicted canonical promoter of *Malat1*[19,20] and approximately 1.4 kb downstream TSS, hereafter referred to as *Malat1*Δ1), and deletion of the 3′-5.7 kb region (hereafter referred to as *Malat1*Δ2), we found that while the *Malat1*Δ1 mutation led to no obvious phenotypic changes, the *Malat1*Δ2 mutant resulted in increased ratio of corneal opacity (15.1% in *Malat1*Δ2 vs 6.6% in WT) and increased cellular senescence in the brain at age of 30 weeks and beyond. Mechanistically, *in vivo* chromatin isolation by RNA purification–mass spectrometry (ChIRP-MS) in young and old mice suggested that *Malat1* interacted with different sets of key aging-related proteins during aging. Our study provides not only a novel mouse model particularly suitable for the mechanistic investigation of aging, but also valuable insights into the biological functions of *Malat1*. We showed *in vivo* evidence that the 3′ conserved region-derived 5.7 kb isoform of *Malat1* (*Malat1_2*), potentially driven by a cryptic internal promoter within the *Malat1* locus, is an essential antioxidant that protects the brain and retina against age-dependent cellular senescence. These findings provide the concrete physiological, unrelated to oncogenic functions of the lncRNA *Malat1*.

RESULTS

Malat1 is upregulated in aged mouse brains as well as senescent MEFs and human iPSC -derived optic cups

Given that the brain is among the organs most susceptible to aging,[8] and that *Malat1* is one of the most abundant lncRNAs in brain tissue, we sought to determine whether it plays a role in aging-related processes. Using the RT-qPCR assay, we found that *Malat1* was significantly upregulated in the brains of old (24 months) mice compared to that of young (1 month) mice and, to a greater extent, in the olfactory bulb (OB) and retina (Figures 1A and S1A). *Malat1* was also upregulated in *in vitro* replicative senescent model systems, including senescent mouse embryonic fibroblasts (MEFs, Figure 1B) and senescent human-induced pluripotent stem cell (iPSC)-derived optic cups, as a retina model (Figure 1C). Although sequences of many known lncRNAs are not conserved,[21] the primary sequence of *Malat1*[22] exhibited high homology across several mammalian species (Figures S1B and S1C). The secondary structures of mouse and human *Malat1* predicted by CROSSalign[23] also showed high similarity (Figure S1D and S1E), implying conserved functions and regulatory mechanisms for *Malat1* between these two species.

Malat1 was previously reported to localize to nuclear speckles.[10] Assays using RNA-FISH with *Malat1* probes in young (P2) and senescent (P7) MEFs showed that *Malat1* mainly localized in the nucleus with no observable cytoplasm signal, and was upregulated during senescence (Figure 1D–1F). These findings concluded that the expression of *Malat1* is upregulated *in vivo* in aged brains (primarily in the OB and retina) and *in vitro* in senescent MEFs and human iPSC-derived optic cups, while its subcellular localization is not altered with senescence.

Malat1 interacts with aging-associated proteins in an age-dependent manner

To map the interactome with *Malat1* at different ages, we performed *in vivo* ChIRP in young and old mouse brains followed by liquid chromatograph-mass spectrometry (LC-MS) analysis, using *LacZ* probes as the negative control. This analysis identified 341 and 72 unique proteins (FDR <1.0 with 95% confidence and LFQ intensity >1 × 10^6) in old and young mouse brains, respectively, indicating a global change in the proteome during aging (Figures S2A and S2B; Table S1 for the complete list). Gene Ontology (GO) analysis of the 341 old brain-enriched proteins showed that they were mainly involved in rRNA binding, structure of ribosomes, and cytoskeletal binding (Figures S2C and S2D), while the 72 young brain-enriched potential *Malat1*-interacting proteins were involved in telomere maintenance, organization, and lengthening (Figures S2E and S2F). These results were in line with previous studies suggesting rRNA expression as a marker for aging[24] while telomere lengthening regulation was associated with high mitotic potential,[25] arguing for an extensive involvement of *Malat1* in aging regulation. Next, we compared our *in vivo* ChIRP-MS results with previous reports and found 21 proteins overlapped with published human *Malat1* CHART-MS[13] and RNA pull-down MS studies[26] (Figure S2G). As repeated evidence from multiple independent studies often associates with high protein identification confidence, we then preferentially focused on validating this panel of proteins. RNA-IP in young and old mouse brains further confirmed that *Malat1*
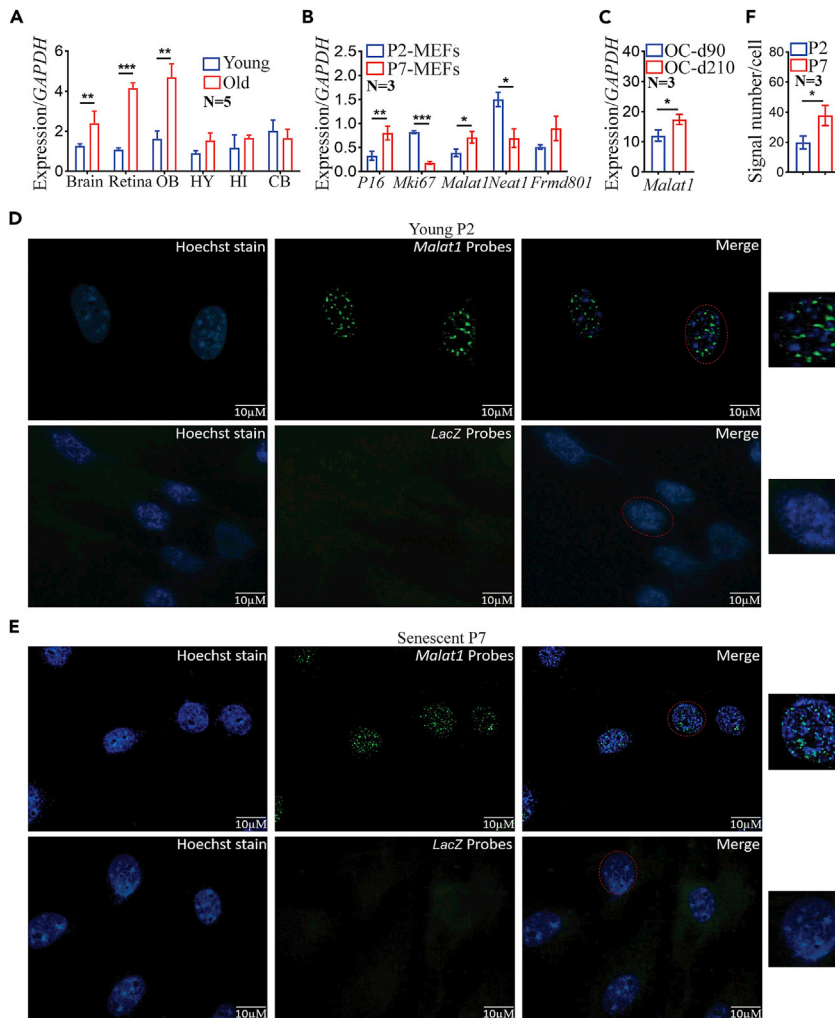
Figure 1. *Malat1* is upregulated with age *in vivo* and *in vitro*

(A) Quantitative reverse transcription PCR (RT-qPCR) assays comparing the relative expression of *Malat1* in young (Y, 1 month) and old (O, 24 months) mouse tissues showed its upregulation in the brain, retina, and OB. OB, olfactory bulb; HY, Hypothalamus; HI, Hippocampus; CB, Cerebellum.

(B) The expression of *P16*[INK4a] and *Malat1* was higher in senescent (P7-MEF) cells, while the expression of *Mki67* and *Neat1* was higher in young (P2-MEF) cells. MEFs, mouse embryonic fibroblasts.

(C) The expression of human *Malat1* in iPSC-derived optic cups (OCs). D-90 and D-210 indicate differentiated optic cups at 90 and 210 days, respectively.

(D–F) RNA-FISH showed *Malat1* localization in Young (D) and senescent MEFs (E). *LacZ* probes were used as negative control for *Malat1* probes. (F) RNA-FISH signal quantification of MEFs. (*$p \leq 0.05$, **$p \leq 0.01$, ***$p \leq 0.001$).

interacted with Nucleophosmin (NPM) in young mouse brains, but with Lamin A/C and hnRNP C in aged mouse brains (Figures 2A–2C). hnRNP C was previously reported to be an interactor of *Malat1 in vitro* by RNA-IP analysis.[27] We confirmed that hnRNP C is a specific *in vivo* interactor of *Malat1* in aged mouse brains, which served as a positive control for our ChIRP-MS analysis. On the other hand, we used 14-3-3e as our negative control as it was similarly enriched by *Malat1* and *LacZ* probes (Figure 2D). Although KAP1 (Trim28) and PHB2 (prohibitin2) did not pass the MS intensity threshold, literature mining indicated that both *Malat1* and KAP1 are involved in myogenic differentiation[28,29] and that knockdown of *KAP1* prevents oncogene-induced senescence.[30] In addition, regulation of prohibitin in the retina is suggested to be related to aging- and diabetes-induced oxidative stress.[31] We thus also included KAP1 and PHB2 in the RNA-IP experiments. The results showed that they indeed interacted with *Malat1* in aged mouse brains (Figures 2E and 2F). To further confirm by another approach, in an independent assay using immortal
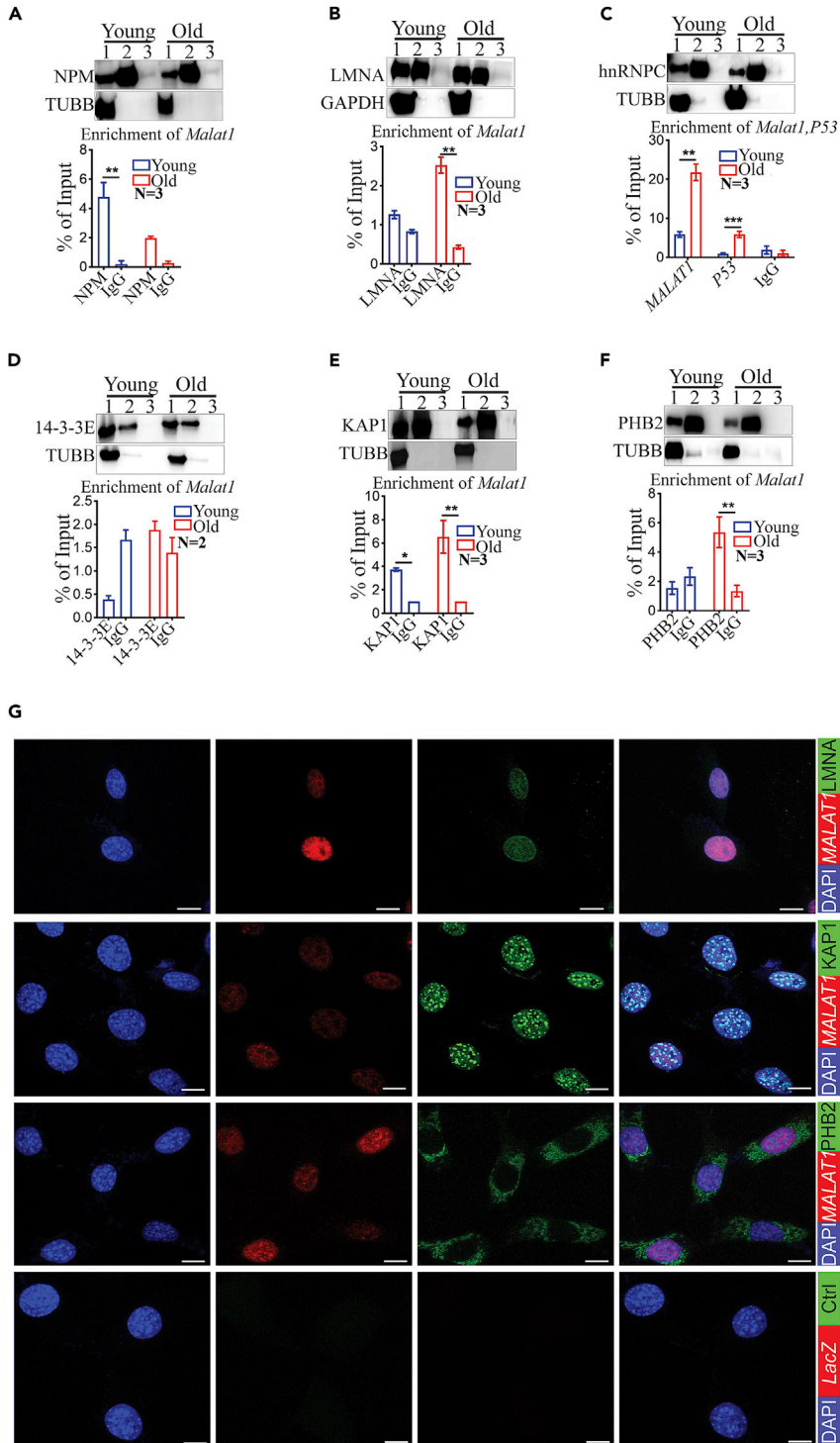
Figure 2. *In vivo* RNA-IP and *Malat1* RNA-FISH combined with immunofluorescence of *Malat1*-interacting proteins

(A–F) RNA-IP of potential *Malat1*-interacting proteins. Immunoblots of *Malat1* RNA-interacting proteins (above) in young and old mouse brains, with RT-qPCR quantification of bound *Malat1* level (below) for (A) NPM-IP, (B) Lamin A/C (LMNA)-IP, (C) hnRNP C-IP, with RT-qPCR quantification of bound *Malat1* and bound P53 mRNA (below), (D) 14-3-3e-IP, which served as our negative control for the MS results, (E) KAP1-IP and (F) PHB2-IP. β-Tubulin (TUBB) or

Figure 2. *Continued*
GAPDH was used as negative control for IP. 1, 2, 3 represent input, IP, IgG samples respectively. *p ≤ 0.05, **p ≤ 0.01, ***p ≤ 0.001.
(G) *Malat1* RNA-FISH combined with immunofluorescence showed co-localization of *Malat1* with LMNA (Lamin A/C) and KAP1. PHB2- showed a cytosolic localization. *LacZ* was used as a negative control.

mouse fibroblast (NIH-3T3) cells, a combined *Malat1* RNA-FISH with immunofluorescence (IF) showed a nuclear co-localization of *Malat1* with Lamin A/C and KAP1 (Figure 2G).

Intriguingly, in addition to the interaction between *Malat1* and hnRNP C in the brains of aged mice, hnRNP C also interacted with the mRNA of P53 (Figure 2C, middle columns), an aging-associated protein and also an upstream regulator of P21. Moreover, we found that in N2A cells, KAP1 interacted with P53 at the protein level in a *Malat1*-dependent manner, since both RNase A treatment and knockdown of *Malat1* using 5 shRNAs abrogated the interaction between KAP1 and P53 (Figures 3A and 3B). In particular, knockdown of *Malat1* in N2A cells led to the downregulation of hnRNPC and upregulation of P53-P21 axis (Figures 3C and 3D), encountering of senescence phenotype with increased positive senescence-associated β-galactosidase (SA-βGal) staining (Figure 3E). These data suggested that *Malat1* interacts with both hnRNP C and KAP1, and that P53 mRNA stability is regulated by hnRNP C and its interaction with KAP1 is *Malat1* dependent.

Among potential *Malat1*-interacting proteins, we selected a group of proteins, focusing on proteins that overlapped with published human *Malat1* CHART-MS and RNA pull-down MS studies, and could be confirmed using RNA-IP assays, including NPM, Lamin A/C, hnRNP C, KAP1, and PHB1/2, for further investigation of their possible involvement in age-dependent expression of *Malat1*. Western blotting results showed that protein expression levels of PHB1, hnRNP C, and KAP1 were significantly upregulated in aged mouse OB and retinas, similar to known aging-associated proteins such as P21, P16, SIRT1, and P53, while PHB2 was only significantly increased in old mouse OB but not retinas (Figures 3F–3I).

In conclusion, the age-associated patterns of expression, binding, and co-localization of these proteins with *Malat1* potentially suggested that *Malat1*, together with these aging associated proteins, might play functional roles in physiological aging processes.

Malat1_1 and *Malat1_2* are independently expressed

Previous studies reported that *Malat1* knockout mice carrying a 3 kb deletion of the 5′-terminus, a poly-A signal inserted immediately downstream of TSS or even whole-length deletion of its gene locus exhibited no obvious phenotypic differences when compared with WT mice. Notably, all of these knockout mice were examined at early ages (6 weeks or earlier).[14–16] Interestingly, although no function has yet been reported for the *Malat1* 3′-region, transcription of the 3′-region persisted despite the 5′-deletion (shown as the mascRNA)[14] or artificially stopping the transcription from its 5′ promoter by inserting a poly-A signal (shown as a 3.2 kb transcript),[15] suggesting the presence of a putative alternative promoter for 3′ *Malat1*. At the same time, 3′ *Malat1* was more conserved than its 5′ (Figure S1C, bottom track). To determine the existence of the *Malat1* 3′ transcript and its biological role through the effects of deletion, we generated *Malat1Δ2* mice by deletion of 5.7 kb from the 3′ part of *Malat1*, the region that was left intact in the previous report of 5′-3 kb knockout mice,[14] leaving only 1.5 kb at the 5′-end of *Malat1* intact (Figure 4A). As a comparison, we also generated *Malat1Δ1* mice carrying a 1.5 kb deletion that consisted of the DNA region left intact in the *Malat1Δ2* mice and the predicted canonical 5′ *Malat1* promoter[19,20] (Figures 4A–4C).

Since previous reports showed persistent expression of 3′ *Malat* transcripts in 5′ *Malat1* deletion mice[14] and poly-A signal insertion induced ablation mice,[15] we examined the relative expression levels of both 5′- 1.5 kb (*Malat1_1*) and 3′- 5.7 kb (*Malat1_2*) *Malat1* isoforms (transcripts) in both knockout model systems generated in this study. Using two or three pairs of primers targeting the 5′ or 3′ *Malat1* deletion regions, we found that in the retinas of *Malat1Δ1* mice, both *Malat1_1* and *Malat1_2* transcripts were significantly reduced compared to WT mice (Figure 4D, red vs. blue columns), although significantly higher levels of *Malat1_2* transcripts were observed compared to *Malat1_1* transcripts (Figure 4D, comparing two red columns). In retinas of mice carrying the *Malat1_2* deletion, transcription from either regions was also significantly decreased when compared to WT (Figure 4D, black vs. blue columns). However, *Malat1_1* transcripts were significantly more abundant than *Malat1_2* transcripts (Figure 4D, comparing two black columns). Thus, *Malat1Δ1* (5′ 1.5 kb deletion) partially abolished *Malat1_2* transcription, while *Malat1Δ2*
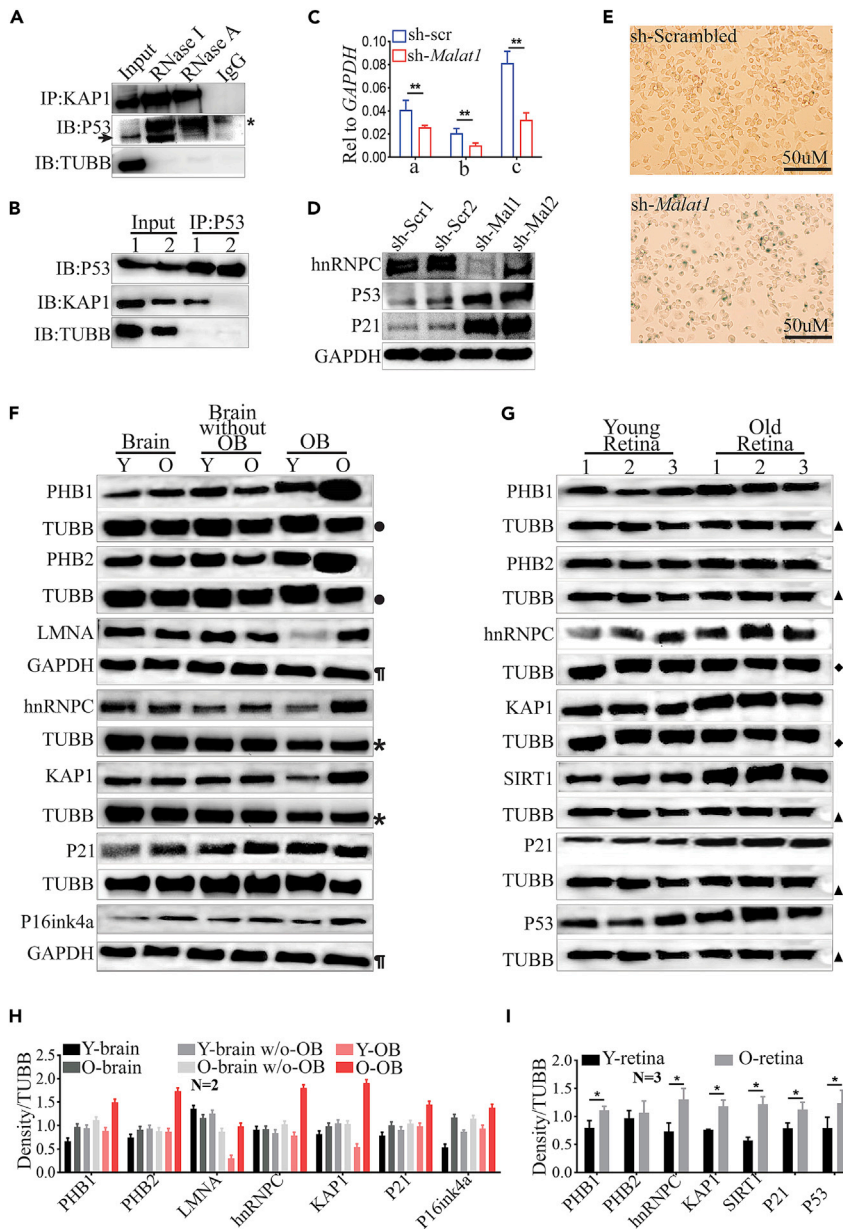
Figure 3. *In vivo* **expression of** *Malat1*-**interacting proteins**

(A–E) *Malat1* mediates KAP1-P53 interaction in N2A cells. (A) KAP1 Co-IP, showing that the interaction between KAP1 and P53 was RNA-dependent (RNase I = RNase inhibitor, RNase A = RNase A). (B) P53 Co-IP showed P53-KAP1 interaction was *Malat1* dependent (1 = shRNA scrambled, 2 = shRNA *Malat1*, *Malat1* was targeted by 5 shRNAs). (C) Quantification of *Malat1* expression in scrambled shRNA (sh-scr) or *Malat1* shRNAs (sh-*Malat1*) transfected N2A cells, by qRT-PCR. (*p ≤ 0.05, **p ≤ 0.01, ***p ≤ 0.001) (a, b, c represented three different *Malat1* specific primer pairs. (D) Western blot of hnRNP C, P53, and P21 in N2A cells transfected with scrambled shRNA (sh-Scr) or *Malat1* shRNAs (5 shRNAs) (sh-Mal). 1 and 2 represneted two biological repeats. (E) Senescence-associated β-galactosidase (SA-βGal) staining of N2A cells transfected with scrambled shRNA or *Malat1* shRNAs (5 shRNAs).

(F–I) Age-dependent expression of potential *Malat1*-interacting proteins. (F) Western blots showed increased expression of PHB1/2, Lamin A/C (LMNA), hnRNP C, KAP1, P21, and P16 in the olfactory bulb (OB) of old mice (Quantification in (H)). (G) Western blots of age-dependent protein expression of potential *Malat1*-associated proteins in the retina showed upregulation of PHB1/2, hnRNP C, KAP1, Sirt1, P53, and P21 in old mouse retinas (quantification in (I)). The different symbols (●, ¶, ★, ◆, ▲) represent different loading controls. The same symbols represent the same loading controls run on the same blot, but were separated and used repeatedly for the purpose of clearly presenting different protein expression patterns.
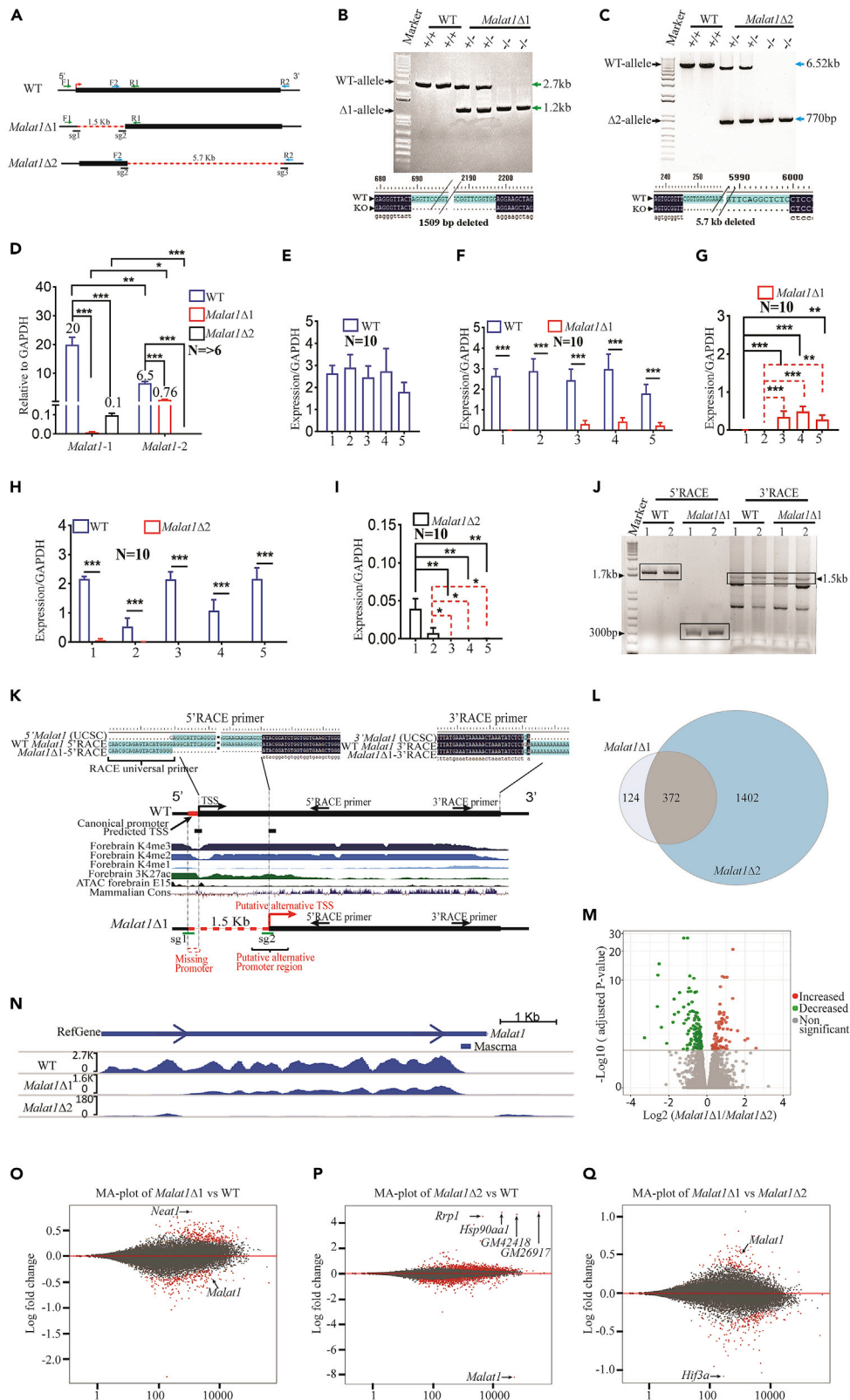
Figure 4. *Malat1*Δ1 and *Malat1*Δ2 mice generation and the independent expression of *Malat1*_1 and *Malat1*_2

(A) Schematic representation of the *Malat1* locus indicating the positions of the sgRNAs used to knockout *Malat1* and the PCR primer sites used for genotyping. horizontal short black lines indicate sg1, sg2, and sg3; green arrows indicate PCR primers F1, R1; blue arrows indicate PCR primers F2, R2; the red arrow indicates Transcription Start Sites (TSS); red dotted lines represent deletion; bold black lines represent WT/remaining transcript.

(B) *Malat1*Δ1 PCR genotyping (F1+R1, lower band 1.2 kb) and Sanger sequencing confirmed a 1509 bp deletion in the *Malat1*Δ1.

(C) *Malat1*Δ2 PCR genotyping (F2+R2, lower band 770 bp) and Sanger sequencing confirmed a 5.7 kb deletion in *Malat1*Δ2.

(D) RT-qPCR assays of *Malat1*_1 and *Malat1*_2 in the retinas of WT, *Malat1*Δ1, and *Malat1*Δ2 mice.

(E–I) RT-qPCR of *Malat1* in the mouse brain. (E) RT-qPCR of *Malat1*_1 and *Malat1*_2 in WT mouse brains. The numbers on the X axis represent primer pairs used. 1 and 2 are for *Malat1*_1 transcript; primers 3, 4, and 5 are for *Malat1*_2 transcript. These are the same for E-I. F) RT-qPCR of *Malat1*_1 and *Malat1*_2 in the *Malat1*Δ1 brain compared to the WT brain. (G) Relative expression of *Malat1*_1 and *Malat1*_2 in the *Malat1*Δ1 brain (data were subtracted from (F)). (H) RT-qPCR of *Malat1*_1 and *Malat1*_2 in *Malat1*Δ2 brain compared to WT brain. (I) Relative expression of *Malat1*_1 and *Malat1*_2 in *Malat1*Δ2 brain (data were subtracted from (H)). *p value ≤ 0.05, **p value ≤ 0.01, ***p value ≤ 0.001.

(J and K) *In vivo* Rapid Amplification of cDNA Ends (RACE). (J) 5′ RACE and 3′ RACE showed persistent expression of *Malat1*_2 in *Malat1*Δ1 retinas. (K) 5′-RACE and 3′-RACE sequence alignment of WT *Malat1* and *Malat1*Δ1 vs *Malat1* cDNA sequence (UCSC). Matched histone marks of forebrain E15 (H3K4me3, H3K4me2, H3K4me1 and H3K27ac) ChIP-seq signals, ATAC-seq signals, and placental mammal conservation data were from the ENCODE database and UCSC, and were presented in the *Malat1* genomic locus. The TSS labeled in black was predicted as described in[32] and the predicted canonical promoter in red color was predicted as described in databases.[19,20] The putative alternative TSS and promoter region were suggested in this study.

(L) Venn diagram of overlapping differentially expressed genes (DEGs) in *Malat1*Δ1 and *Malat1*Δ2 compared with WT mouse brains, respectively.

(M) A volcano plot of DEGs in *Malat1*Δ1 and *Malat1*Δ2 compared with WT mouse brains respectively.

(N) RNA-seq reads around the *Malat1* locus, in WT, *Malat1*Δ1, and *Malat1*Δ2 mouse brains showed an independent expression of *Malat1*_1 and *Malat1*_2 transcripts.

(O–Q) 2D MA-Plot (a method to show gene expression changes among different groups) for DEGs identified from RNA-Seq. (O) MA-plot of DEGs in *Malat1*Δ1 compared to WT mouse brains showed a significant decrease of *Malat1* and significant upregulation of *Neat1*. (P) MA-plot of DEGs in *Malat1*Δ2 compared to WT mouse brains showed a significant decrease of *Malat1* and global DEGs independent of *Neat1*. (Q) MA-plot of DEGs in *Malat1*Δ1 compared to *Malat1*Δ2 mouse brains showed a significant upregulation of *Malat1* (*Malat1*_2 transcript).

(3′ 5.7 kb deletion) partially abolished *Malat1*_1 transcription. These results indicated that although transcription from either region decreases in the absence of the counterpart, separate regulatory elements might independently drive the expression of either region. These data led us to scrutinize the expression differences in *Malat1*_1 and *Malat1*_2 isoforms in WT mice using the same primer sets as described above. Surprisingly, *Malat1*_1 and *Malat1*_2 were differentially expressed to a great extent in retinas of WT mice (Figure 4D, comparing two blue columns), but not in brain tissues (Figure 4E), although patterns of transcription of both *Malat1*_1 and *Malat1*_2 in the brain recapitulated the expression patterns in retina tissue of both knockout lines (Figures 4D and 4F–4I).

Northern blot analysis did not detect partial *Malat1* transcripts in either *Malat1*Δ1 or *Malat1*Δ2 mouse brains (Figure S3A), likely due to their low levels of expression. However, rapid amplification of cDNA ends (RACE) assays showed persistent expression of both the 5′ and 3′ ends of the 5.7 kb *Malat1*_2 transcripts, suggesting the existence of the full-length 5.7 kb transcript, in *Malat1*Δ1 retina (Figure 4J) and brain (Figures S3B–S3D), implying that the 3′ 5.7 kb transcripts (*Malat1*_2) of *Malat1* might still execute function when the 5′ 1.5 kb region of *Malat1* was deleted. In addition, sequencing of the 5′ RACE products amplified in the *Malat1*Δ1 mice revealed that the 5′ end of the *Malat1*_2 transcript overlapped exactly with the promoter-associated epigenetic markers such as histone H3K4me3 peaks identified from the ChIP-Seq data in ENCODE, suggesting that its independent transcription is potentially driven by a putative alternative promoter within the *Malat1* locus (Figure 4K).

Respective *cis*- and *trans*-regulatory activities of *Malat1*_1 and *Malat1*_2

To better understand the global transcriptional changes in *Malat1*Δ1 and *Malat1*Δ2 mice, we performed RNA-Seq using brain tissues from knockout and WT mice. We identified 1402 differentially expressed genes (DEGs) specific to *Malat1*Δ2 mice and 124 DEGs specific to *Malat1*Δ1 mice, with 372 overlapping DEGs shared between the two knockout models (Figure 4L), and a volcano plot showed the DEGs in *Malat1*Δ1 and *Malat1*Δ2 mice (Figure 4M). Principal component analysis and hierarchical clustering were
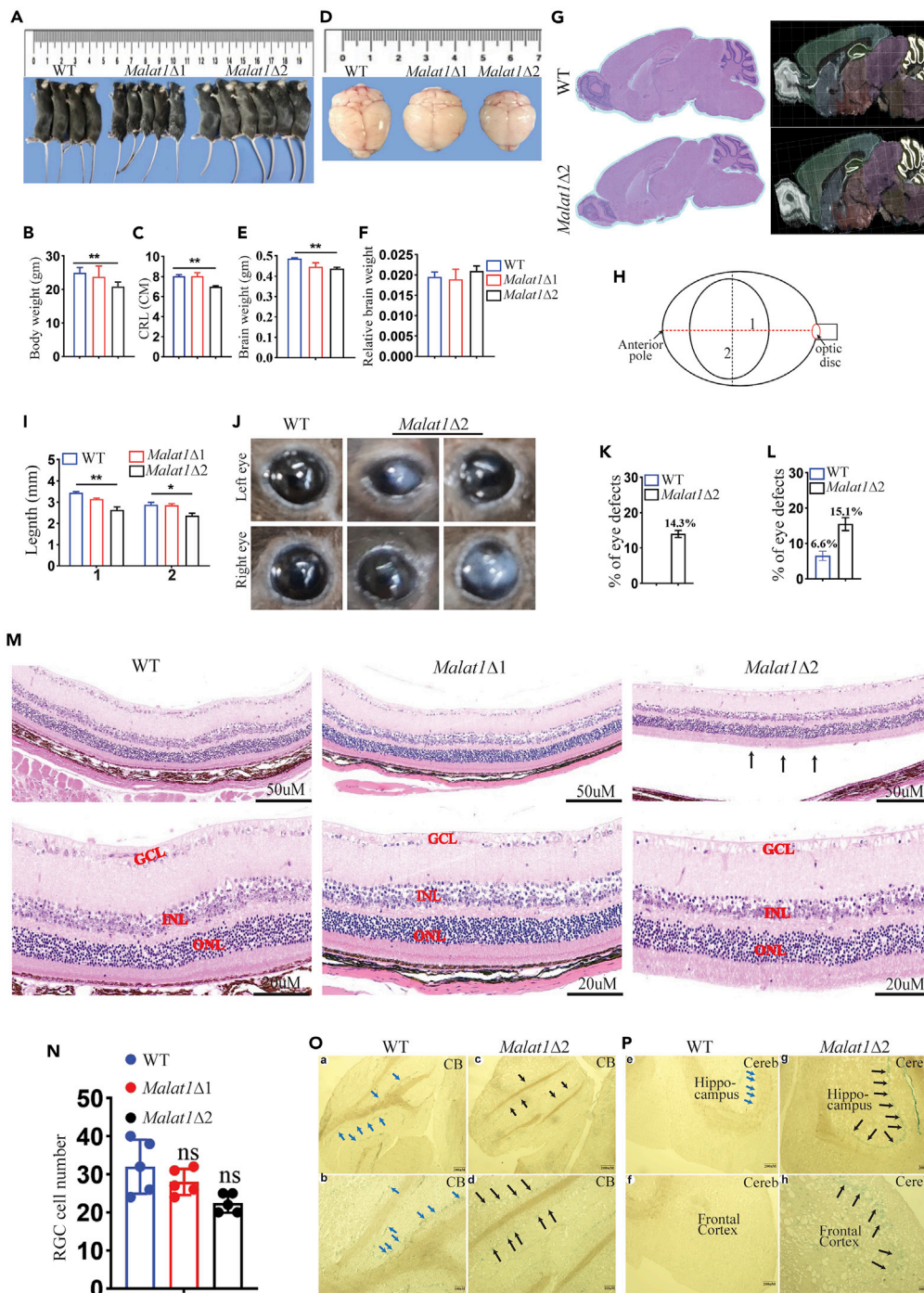
Figure 5. Age-associated phenotypes of *Malat1*Δ1 and *Malat1*Δ2 mice

(A–C) Gross morphometric measurements of *Malat1*Δ1 and *Malat1*Δ2 mice at the age of 8 weeks old. (A) Gross macrograph of WT, *Malat1*Δ1, and *Malat1*Δ2, and quantification of the body weights (B) crown rump length (CRL) (C).

(D) Gross brain macrograph of WT, *Malat1*Δ1, and *Malat1*Δ2 mice.

(E and F) Quantification of the absolute brain weight (E) and relative brain weight (F).

(G) Cross histological section of WT and *Malat1*Δ2 brains (Left), and Allen brain atlas (right) showed no differences in 50-week-old mice.

(H) Schematic of eyeball axial length (1) and sagittal length (2) and their quantifications in (I).

Figure 5. *Continued*

(J) Representative *in situ* gross macrograph of eye balls at the age of 30 weeks (Left eyes on top, and Right eyes on bottom).

(K) Percentage of eye defects at 8–9 months of age.

(L) Percentage of eye defects at the age of 8–13 months. In B, C, E, F, and I, blue columns were WT, red columns were *Malat1*Δ1, and black columns were *Malat1*Δ2. *p value ≤ 0.05, **p value ≤ 0.01.

(M) Cross sectional retinas with H&E staining in WT, *Malat1*Δ1, and *Malat1*Δ2 mice. *Malat1*Δ2 retinas showed a fewer cells in the ganglionic cell layer (GCL). Black arrows represent retinal detachment. INL= inner nuclear layer.

(N) GCL count quantification.

(O) Photo-micrographs of SA-βGal stained 10-month WT (a and b) and *Malat1*Δ2 (c and d) mouse cerebellum, with limited staining among Purkinje cells.

(P) Photo-micrographs of 10-month mouse cerebrum, hippocampus, and frontal cortex. WT (e and f) showed no SA βGal staining, and *Malat1*Δ2 (g and h) showed clear SA βGal staining of hippocampus and frontal cortex (CB = Cerebellum, and Cereb = Cerebrum). Blue and black arrows show the same regions in WT and KO.

conducted for data comparison and visualization using the ClustVis R package[33] (Figures S4A–S4C). As observed in our RT-qPCR data shown above, RNA-Seq results confirmed the complete absence of *Malat1*_1 transcripts in *Malat1*Δ1 samples, and likewise no *Malat1*_2 transcripts among the reads from *Malat1*Δ2 mice. However, there was still expression of the *Malat1*_2 in *Malat1*Δ1 mice, although decreased (Figures 4N–4Q, and Tables S2, S3, S4). The heatmaps of genes with differential expression in *Malat1*Δ1 and *Malat1*Δ2 were presented in Figure S4D–S4F. These data thus suggested that the 5.7 kb *Malat1*_2 transcripts we identified in the absence of the predicted canonical 5′ promoter in the *Malat1*Δ1 mice could be driven by a different promoter from the one driving *Malat1* 5′ end transcription. Alternatively, we could not exclude the possibility that the remaining 5.7 kb transcript was still driven by the upstream regulatory sequences located upstream of the 5′ 1.5 kb region of *Malat1*. Notably, the transcription of *Malat1*_1 and *Malat1*_2 both proceeded in an ostensibly quasi-dependent manner, showing that *Malat1*Δ1 and *Malat1*Δ2 could lead to a decrease in the expression of their respective counterpart regions.

Among the top 10 DEGs, *Neat1*, a conserved lncRNA-located ∼40 kb upstream of *Malat1* was observed in much higher abundance in *Malat1*Δ1 mice than WT (Figure 4O). We subsequently validated the differential upregulation of *Neat1* in *Malat1*Δ1 mice using RT-qPCR (Figure S4G). This finding aligned with previous research characterizing the outcomes of deletion of 5′ *Malat1*,[14] supporting the notion that 5′ *Malat1* transcripts function as negative *cis*-regulators of *Neat1* (Table S4). Additionally, GO analysis of *Malat1*Δ1 DEGs showed that genes involved in the regulation of synapse assembly, structure, and synaptic vesicle transport were significantly upregulated in these mice (Figures S5A–S5C), while a number of genes involved in ribosomal biogenesis, translation initiation, and protein localization to the endoplasmic reticulum were differentially downregulated (Figures S5D–S5F). In contrast to *Malat1*Δ1, none of the top 400 DEG hits identified in the brain tissue of *Malat1*Δ2 mice were transcribed from loci within 1500 kb of either end of *Malat1*. Collectively our data indicated that the *Malat1*_1 and *Malat1*_2 transcripts participate in or act in *cis*- and *trans*-regulation, respectively. Most notably, *Malat1*Δ2 altered the expression of many more genes in the mouse brain. Moreover, GO analysis revealed enrichment for upregulated DEGs related to ribosomal biogenesis, ribosome assembly, and ribonucleoprotein complex biogenesis in *Malat1*Δ2 (Figures S5G–S5I and S5M), while the downregulated DEGs were enriched for embryonic eye morphogenesis, regulation of neuroblast proliferation, and neuronal cell differentiation (Figures S5J–S5M). Together with the fact that the *Malat1*_2 transcript region had higher sequence conservation than the *Malat1*_1 transcript region, these findings indicated that *Malat1*_2 transcripts might function in the regulation of a larger scope and wider range of genes than *Malat1*_1 transcripts. Specifically, deletion of the *Malat1*_2 transcript region might lead to a global loss of proteostasis, a hallmark of aging.

*Malat1*Δ2 mice exhibit increased cellular senescence and oxidative stress in the retina

Notably, all previously reported *Malat1* knockout mice were examined at early ages (6 weeks or earlier) and did not exhibit phenotypic differences when compared with WT mice.[14–16] Thus, we sought to examine our *Malat1*Δ1 and *Malat1*Δ2 phenotypes at both young and old ages.

In *Malat1*Δ2 mice, we observed a reduction in body weight and crown rump length (Figures 5A–5C), and absolute brain weight without changes in the relative brain weight compared to WT mice at the age of 8 weeks old (Figures 5D–5F). In contrast, we did not observe significant changes in the *Malat1*Δ1 mice

compared to WT mice (Figures 5A–5F), which was consistent with previous reports.[14] In addition, we did not observe any histological changes in the brains of *Malat1*Δ2 mice at the age of 50 weeks (Figure 5G).

The age-dependent accumulation of senescent cells in the nervous system accelerates neurodegeneration,[34] which is most clearly manifested in the retina, an extension of the nervous tissue outside the brain, due to the high sensitivity to physiological and pathological stresses.[35] Previous studies have shown that retinal cells do not divide under normal conditions, and such withdrawal from the cell cycle might increase the likelihood of early tissue aging.[36,37] Hence, the retina is an appropriate indicator of neurodegenerative diseases[38–40] and healthy brain aging.[41,42] During their lifetime, the macula undergoes significant degenerative changes, leading to visual decline and often visual loss.[43] In mice, several age-associated changes in the eye, including cataracts[44] and age-associated atrophy of the retina after histologically normal development, are also observed as an aging phenotype.[45] In addition, oxidative stress was previously reported to initiate ocular injury, resulting in decreases in visual acuity or vision losses in severe cases.[46] Retinal alterations have been reported in patients with neurological disorders such as stroke, multiple sclerosis, Parkinson disease, and Alzheimer disease.[47,48] On the other hand, clearance of senescent cells in the body improves late-life health and delays age-associated frailty in mice.[49,50]

We thus further examined the phenotype of *Malat1*Δ2 mice after 30 weeks of age and observed a decrease in ocular dimensions (Figures 5H and 5I). Specifically, 14.3% of *Malat1*Δ2 mice from both sexes exhibited ocular phenotypes (Figures 5J and 5K), including cataracts and corneal opacity (of at least one eye), while after 53 weeks of age the percentage was 15.1% for *Malat1*Δ2 mice compared to 6.6% for WT mice (Figure 5L). Histological examination showed a decrease in the ganglionic cell layer, although no statistically significant changes were observed at the age of 10–12 months (Figures 5M and 5N). *Malat1*Δ2 mice also exhibited higher positive SA-βGal staining in the hippocampus and frontal cortex at 10 months of age than WT control mice (Figures 5O and 5P). On the other hand, we did not observe any histomorphological changes in the brain (data not shown). These findings suggested that the 3′ region of *Malat1* is indispensable for retinal aging.

Malat1_2 transcript regulates aging-associated proteins and induces P21 mRNA and protein expression

To examine whether *Malat1*Δ1 or *Malat1*Δ2 regulates the *in vivo* expression of *Malat1*-interacting proteins identified above, we conducted Western blotting analysis on a panel of *Malat1*-interacting proteins in *Malat1*Δ1 and *Malat1*Δ2 mice. We found that compared to WT mice, Lamin A/C (LMNA), hnRNP C, PHB1, and PHB2 were significantly downregulated, while NPM was upregulated in brain tissues of *Malat1*Δ2 mice (Figures 6A and 6C for quantification). Most of these proteins exhibited the same expression pattern in the retina of *Malat1*Δ2 mice compared to WT mice (Figures 6B and 6D for quantification). In particular, KAP1 was downregulated in both the retina and brain of *Malat1*Δ2 mice, although only significantly so in the retina (Figures 6A–6D). In general, *Malat1*Δ1 had less impact on the expression of corresponding proteins than *Malat1*Δ2.

Previous studies suggest that *Malat1* can regulate Sirt1 through its interaction with Lamin A/C, which is a prerequisite for Sirt1 activation.[51] We found that Sirt1 was significantly downregulated in the brain and retina of *Malat1*Δ2 mice (Figures 6A–6D), probably due to the downregulation of Lamin A/C. NPM was previously shown to form a complex with Sox2 to maintain embryonic stem cell pluripotency and differentiation.[52] Sox2 thus serves as a marker for functional pluripotency of neural precursor cells (NPCs), which is required to maintain the expression of Lin28. Sox2-Lin28 interaction mediates NPCs proliferation and neurogenic potential.[53] We therefore also checked the changes in the expression of Sox2 and Lin28 in the brains of *Malat1*Δ2 mice and found that both were significantly downregulated (Figures 6A–6D), supporting that the 5.7 kb deletion of 3′ *Malat1* leads to the dysregulation of Sox2 and Lin28, potentially mediated by NPM.

Due to our observations of the *Malat1*-dependent interaction between P53 and KAP1 (Figures 3A and 3B), as well as the reported P53-dependent regulation of P21, we further examined the expression of P53 and P21 in *Malat1*Δ1 and *Malat1*Δ2 mice and found that P53 was significantly downregulated in the retina of *Malat1*Δ2 mice, but not significantly in *Malat1*Δ2 or *Malat1*Δ1 mouse brains (Figures 6A–6D). Coincidentally, P53 mRNA stability also decreased in *Malat1*Δ2 NIH3T3cells (Figure 6E). In contrast, P21 appeared upregulated in both the brain and retina of *Malat1*Δ2 mice (Figures 6A–6D), which could be partially
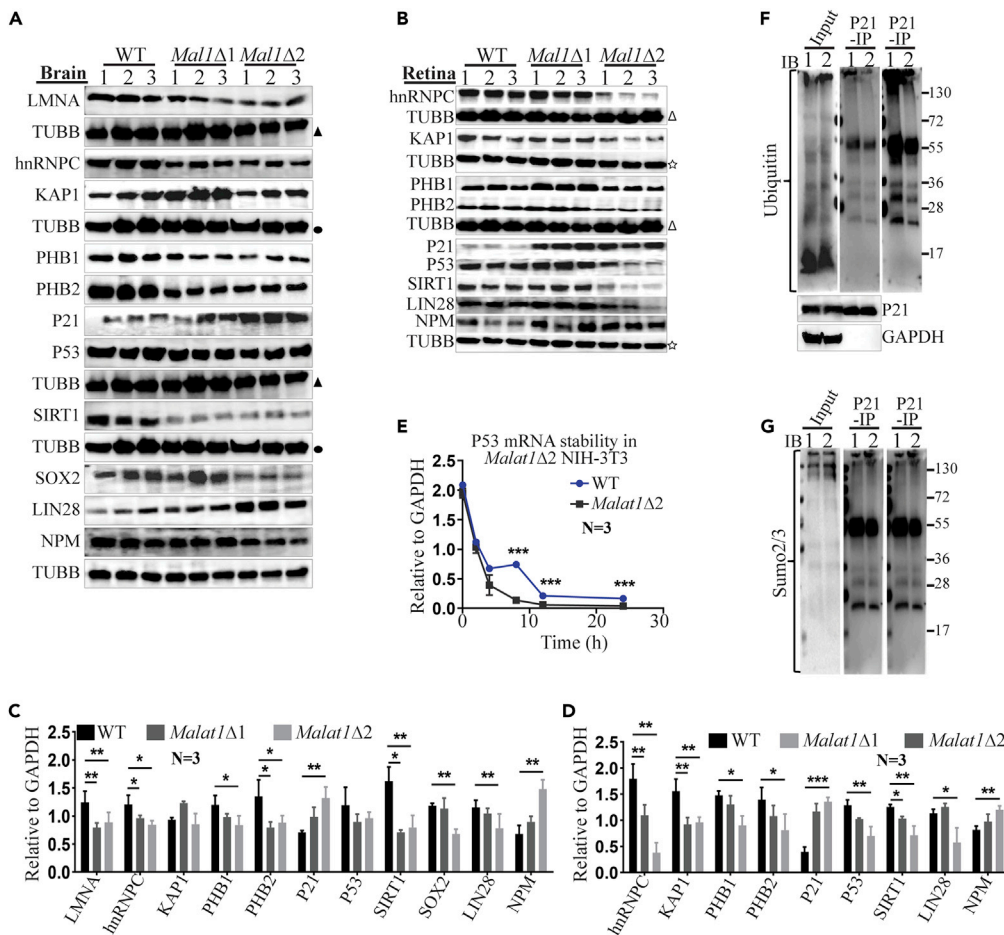
Figure 6. *Malat1*Δ2 mutant mice show increased P21 and decreased P53 expression

(A–D) Western blots of *Malat1*-associated protein expression patterns in the brain and retina. (A) Brain Lamin A/C (LMNA), hnRNP C, PHB1, PHB2, Sirt1, Sox2, and Lin28 were significantly downregulated, P21, and NPM were significantly upregulated, while KAP1 was not significantly changed. The numbers at the top of each well indicated biological replicates, and quantification was shown in (C). (B) Retina P21 and NPM were upregulated, while hnRNP C, KAP1, PHB1, PHB2, P53, Sirt1, and Lin28 were all downregulated. Similarly, the numbers at the top of each well indicated biological replicates, and quantification was shown in (D). The different symbols (▲, ●, Δ et al.) represent different loading controls. The same symbols represent the same loading controls run on the same blot but were separated and used repeatedly for the purpose of clearly presenting different protein expression patterns.

(E) P53 mRNA stability in *Malat1*Δ2 NIH3T3 cells.

(F) P21 ubiquitination in WT and *Malat1*Δ2 mouse brains. 1 represents WT, 2 represents *Malat1*Δ2. The data showed that the levels of P21 ubiquitination in *Malat1*Δ2 were lower than those in WT.

(G) P21 sumoylation in WT and *Malat1*Δ2 mouse brains. 1 represents WT, 2 represents *Malat1*Δ2, showing that the levels of P21 sumoylation in *Malat1*Δ2 were similar to those in WT.

In (F and G), the middle panels were lower exposure, the right panel were higher exposure, and the same loading control was represented in (F).

explained by the downregulation of P53 at both the mRNA and protein levels due to the loss of *Malat1* and its interacting partner hnRNP C. On the other hand, P21 expression may also be regulated in a P53-independent manner,[54] and the induction of NPM we observed in *Malat1*Δ2 mice might promote the stability of P21 mRNA, consistent with previous reports.[55]

Although the mechanisms governing P21 protein stability have not been fully illustrated, ubiquitination of P21 is generally believed to be a destabilizing factor, while sumoylation is a stabilizing factor.[56–58] Having confirmed the upregulation of P21 expression in the brain and retinal tissues of *Malat1*Δ2 mice, as well as with RNA-Seq data (data not shown), we then checked the ubiquitination and sumoylation of P21 in the

brains of the same panel of mice. Remarkably, P21 ubiquitination was significantly decreased, as detected using specific antibodies (Figure 6F), while its sumoylation level did not significantly change in the *Malat1*Δ2 brain (Figure 6G). Collectively, our data indicated that P21 is stabilized at both the mRNA and protein levels in *Malat1*Δ2 mice, likely due to the deletion of the 5.7 kb 3′ *Malat1*, which is coincident with the increased cellular senescence and oxidative stress in the brain and retina of these mice.

DISCUSSION

Through targeted deletion of a 5′ 1.5 kb fragment (*Malat1*Δ1) and a 3′ 5.7 kb region (*Malat1*Δ2) of *Malat1* in mice, we found that the deletion of 3′ conserved region-derived 5.7 kb transcript (isoform) of *Malat1* (*Malat1_2*) is associated with increased oxidative stress in the eye and increased cellular senescence in the brain during mouse aging process. ChIRP-MS suggested that *Malat1* differentially interacts with key aging-related proteins in young and old mice, providing insights into the underlying mechanism for the observed phenotypes.

Eissmann et al. generated *Malat1* knockout mice using homologous recombination[59,60] and the Cre-loxp system to show that the full-length deletion of *Malat1* in mice leads to no observable phenotypes or histological abnormalities within the age of 6 weeks.[16] However, they did note a moderate increase in *Neat1* expression in the lungs, colon, kidneys, and brain. Zhang et al. also showed upregulation of *Neat1* in livers and brain cortices.[14] The no-phenotype detected in the above two reports (whole length or 5′ partial deletion of *Malat1*) might be attributable to the compensation of *Malat1* function through the upregulation of the nearby *Neat1* lncRNA, whose expression was not changed compared to WT in our *Malat1*Δ2 mice (which had increased oxidative stress and cellular senescence phenotypes), but was upregulated in *Malat1*Δ1 mice (had no phenotypes). We also noted that previous studies were performed only in young mice, missing examinations in older mice. Coincidentally, upregulation of *Neat1* in Huntington disease pathogenesis suggests its neuroprotective role during neuronal injury.[61] Moreover, a study crossing full-length *Malat1* deletion mice with *Apoe1* knockout mice suggested a negative regulatory role of *Malat1* in the vascular endothelium.[62] On the other hand, aging-associated pathologies such as atherosclerosis, significantly increase cytokine production[62] and reduce vascular endothelial cell proliferation[63] in crossed littermates of full length *Malat1* knockout mice and *Apoe1* knockout mice, suggesting a protective role of *Malat1* as an anti-aging lncRNA.

In mice, several age-associated changes of the eye, including cataracts,[44] and age-associated atrophy of the retina after histologically normal development are also considered as aging phenotypes.[45] The thickness of the whole retina in aged mice is markedly decreased in both peripheral and central areas, and the loss of ganglion cells in the retinas of senescence acceleration mice is greater than that in WT mice at all ages.[64–66] This means that accelerated senescence improves the rate of loss of ganglion cells in retinas. Consistently, we found that the retinas of *Malat1*Δ2 mice became thinner and easily detached compared to WT mice. The retinas of *Malat1*Δ2 mice also showed reductions in the ganglionic cell layer at 10–12 months of age. In addition, we showed that Sirt1, reported to localize to the cornea, lens, iris, ciliary body, and retinas,[67] was significantly downregulated in the retina and brain of our *Malat1*Δ2 mice. Furthermore, the same study showed that *Sirt1* knockout mice exhibit a prematurely aged ocular phenotype, consistent with other published work showing that downregulation of the lin28-Sox2 axis fails to maintain retinal stem cell regeneration.[67] It has also been suggested that *Malat1* can regulate Sirt1 through its interaction with Lamin A/C, which is a prerequisite for Sirt1 activation.[51] Taken together, these findings support that 3′ conserved region-derived 5.7 kb isoform of *Malat1* (*Malat1_2*) may confer a potent, protective effect against aging in ocular tissue.

In addition to the above-mentioned two reported *Malat1* knockout models, the Prasanth KV group also generated *Malat1* knockout mice, carrying an insertion of the lacZ reporter gene followed by polyadenylation signals immediately downstream from the TSS, and found that a 3.2 kb 3′ *Malat1* RNA still exists in the brain tissues with no apparent phenotypes observed.[15] Again, only mice at a young age were examined. Interestingly, the Spector DL group (Zhang B et al., 2012) reported trace amounts of mascRNA (∼60 nt) remaining in the brains of *Malat1* knockout mice carrying a 3 kb deletion at the 5′ terminus.[14] Consistently, our *Malat1*Δ1 mice, in which the 1.5 kb region containing the predicted canonical promoter upstream TSS (100 bp) and 1.4 kb region downstream TSS were deleted, also exhibited reduced but persistent expression of *Malat1_2* without showing obvious phenotypic differences when compared to WT mice. These results collectively imply that *Malat1_2* transcripts, detected in both Prasanth KV knockout mice and *Malat1*Δ1 mice, although at a lower level, are

potentially driven by a putative alternative promoter for independent transcription, and maintain the physiological functions of *Malat1*. Remarkably, *Malat1*Δ2 mice distinguished from *Malat1*Δ1 mice for increased oxidative stress and senescence pathologies in the brain and retinas, indicating that this 3′ isoform of *Malat1* (*Malat1_2*) with relatively higher sequence conservation is essential for the timing and progression of several developmental processes related to brain and retinal aging.

In support of our phenotypic and molecular observations, transcriptomic analysis of *Malat1*Δ2 mice revealed that notable of downregulated genes were involved in regulating eye development and differentiation of neural stem cells, while some of the upregulated genes were involved in ribosomal biogenesis and assembly, factors thought to accelerate premature aging. This notion is further supported by enhanced atherosclerosis and increased cytokine production in *Malat1*$^{-/-}$*Apoe1*$^{-/-}$ mice,[62] both of which are aging-associated.

While we observed cytosolic localization of PHB2 in NIH3T3 cells and thus did not co-localize with the nuclear localized *Malat1* (Figure 2G), PHB2 was previously reported to localize in the nuclei of the retina, decrease with aging, and further translocate to the cytosol upon H_2O_2 treatment.[31] It has been previously reported that *Malat1* is involved in the translocation of hnRNP C;[27] thus, our data might suggest a potential similar function for PHB2, and this need to be further studied.

Ribosomal biogenesis has been previously linked to aging and its repression has resulted in an increased life span in *Caenorhabditis elegans*, *Drosophila*, *Saccharomyces cerevisiae*, and mice, as well as in humans.[68] Therefore, enhanced ribosomal biogenesis is generally believed to accelerate aging. Consistent with this idea, upregulated ribosomal biogenesis along with abnormally large nucleoli has been observed in senescent fibroblasts isolated from patients suffering from the premature aging disease Hutchinson-Gilford progeria.[69,70] Enhanced ribosomal biogenesis is accompanied by an increased rate of protein translation, leading to an upregulation of protein synthesis and global disruption of proteostasis, a hallmark of aging.[71,72] Additionally, caloric restriction, which has been shown to promote longevity, leads to the downregulation of ribosomal biogenesis through several mechanisms.[73,74]

The upregulation of ribosomal biogenesis and assembly in *Malat1*Δ2 mice in our study might reflect interaction between *Malat1* and NPM, which is involved in rRNA cleavage, transcription, and nuclear export of RPL5.[75,76] This protein is also reported to participate in the regulation of Sirt1, as a component of the energy-dependent nucleolar silencing complex (eNoSC) that is responsible for the epigenetic silencing of rDNA gene expression,[73] the downregulation of which leads to rDNA transcription.

Our data also showed that *Malat1* specifically interacts and co-localizes with several age-associated proteins such as Lamin A/C, hnRNP C, and KAP1. The 5.7 kb deletion of 3′ *Malat1* also downregulated the expression of Rab7a (data not shown) which may lead to microglial cell senescence and deteriorated brain conditions. For example, it has been shown that Rab7a conditional knockout mice develop a massive accumulation of lipofuscin granules in microglia as early as nine months of age, accompanied by accelerated microglial senescence and compromised myelin sheath regeneration.[77] In addition, the downregulation of P53 protein levels in the retinas of *Malat1*Δ2 mice suggests that *Malat1* may contribute to P53 stability through direct interaction with hnRNP C in the brains of aged mice.

There is also a possibility that DNA elements localized in the 3′ region of *Malat1* may influence the aging process through interactions with specific functional DNA elements or proteins. Rescue experiments will help to investigate how *Malat1* regulates its associated proteins and whether there is a functional DNA element in the 3′ region of *Malat1*.

In conclusion, deletion of the 3′ region (5.7 kb) of *Malat1* in mice leads to a wide range of molecular consequences, including downregulating potent antioxidants PHB1 and PHB2,[31] potentially sensitizing the brain to oxidative stress; downregulating Sox2/Lin28 in the retina and brain, which likely maintain and renew adult retinal and brain stem cells; and upregulating NPM while downregulating Sirt1, potentially increasing P21 stability and enhancing ribosomal biogenesis.

Through individual targeted knockouts of *Malat1*Δ1 and *Malat1*Δ2, we thus provide *in vivo* evidence for the concrete physiological functions of *Malat1* as a potent lncRNA for the regulation of aging-related

processes, and that the loss of the 3′ region (5.7 kb) of *Malat1* leads to accelerated senescence, an oxidative stress phenotype in the retina and visual impairment. We showed that the 3′ 5.7 kb isoform of *Malat1* with relatively higher sequence conservation might regulate over a thousand genes *in trans*, whereas the 5′ 1.5 kb transcripts of *Malat1* might regulate *Neat1* and other genes in an *in cis* manner.

Despite increased expression of PHB1/2, SIRT1, and Lamin A/C during aging, *in vivo* loss of their functions was associated with accelerated aging and premature death, suggesting that these proteins play an anti-aging role. On the other hand, P21 was upregulated with aging, and removing P21 positive cells improved late-life health. Therefore, we hypothesize that *in vivo* upregulation of *Malat1* and its interacting proteins, potentially via mechanisms involving P53, might function to counter aging effects. This can explain why the downregulation of *Malat1_2* and consequently its partners resulted in increased oxidative stress in mouse retinas. Furthermore, P21 is a key driver of aging that shows increased expression in old mouse brains and *Malat1Δ2* knockout mice. While the underlying molecular mechanisms warrant further investigation, our findings strongly argue that the lncRNA *Malat1* is an essential sensor lncRNA that can regulate a hub of proteins indispensable for physiological aging.

This work thus provides not only a novel mouse model particularly suited for mechanistic dissecting of the aging process, but also a substantial foundation for further study of the biological role of *Malat1* as a regulator of aging processes.

Limitation of the study

In this study, we mainly focused on exploring the physiological role of the highly conserved 3′-termnius of the lncRNA *Malat1* in physiological aging, and generated a unique mouse model that can be used to explore its biological role in different pathophysiological conditions. More experiments need to be performed to reveal the underlying mechanisms using the *in vivo* model.

STAR★METHODS

Detailed methods are provided in the online version of this paper and include the following:

- KEY RESOURCES TABLE
- RESOURCE AVAILABILITY
  - Lead contact
  - Materials availability
  - Data and code availability
- EXPERIMENTAL MODEL AND SUBJECT DETAILS
  - Ethics committees statement
  - Mouse models
- METHODS DETAILS
  - Cell culture and transfection
  - Immunoblotting and western blot
  - Co-immunoprecipitation
  - Quantitative reverse transcription PCR (RT-qPCR)
  - *In vivo-* ChIRP
  - Mass spectrometry sample preparation
  - Mass spectrometric analysis and database search
  - Ubiquitination and Sumoylation assays
  - RNA fluorescence *in situ* hybridization (RNA FISH)
  - RNA immunoprecipitation assay
  - Northern blot and densitometry analysis
  - mRNA stability assay
  - Retinal histology
- QUANTIFICATION AND STATISTICAL ANALYSIS

SUPPLEMENTAL INFORMATION

Supplemental information can be found online at https://doi.org/10.1016/j.isci.2022.105740.

AUTHOR CONTRIBUTIONS

A.R.G. and X.S. designed the experiments. A.R.G. performed most of experiments. S.W.K. performed RACE, confirmed RNA-Seq data by RT-qPCR, maintained KO mice, confirming KO mice phenotypes and helped with figure preparation. R.E., Z.R., and C.Y.X. carried out the RNA-Seq analysis. S.J.W. and Yong Z performed the MS and analysis. S.Q.W. performed the IF-RNA FISH. M.W. helped with dissection of the mouse retinas under the supervision of T.X. C.J. analyzed the ChIRP-Seq data and edited the figures. W.G.L. edited the figures extensively. Yan Z and Z.Z. provided useful suggestions and edited the manuscript. X.S. supervised the entire study and analyzed the data with A.R.G. and S.W.K. A.R.G., S.W.K., Yong Z., and X.S. wrote the manuscript.

DECLARATION OF INTERESTS

All the authors declare no competing interests.

REFERENCES

1. Payre, F., and Desplan, C. (2016). RNA. Small peptides control heart activity. Science *351*, 226–227. https://doi.org/10.1126/science.aad9873.

2. Wilusz, J.E., Sunwoo, H., and Spector, D.L. (2009). Long noncoding RNAs: functional surprises from the RNA world. Genes Dev. *23*, 1494–1504. https://doi.org/10.1101/gad.1800909.

3. Kapranov, P., Cheng, J., Dike, S., Nix, D.A., Duttagupta, R., Willingham, A.T., Stadler, P.F., Hertel, J., Hackermüller, J., Hofacker, I.L., et al. (2007). RNA maps reveal new RNA classes and a possible function for pervasive transcription. Science *316*, 1484–1488. https://doi.org/10.1126/science.1138341.

4. Derrien, T., Johnson, R., Bussotti, G., Tanzer, A., Djebali, S., Tilgner, H., Guernec, G., Martin, D., Merkel, A., Knowles, D.G., et al. (2012). The GENCODE v7 catalog of human long noncoding RNAs: analysis of their gene structure, evolution, and expression. Genome Res. *22*, 1775–1789. https://doi.org/10.1101/gr.132159.111.

5. Guttman, M., Amit, I., Garber, M., French, C., Lin, M.F., Feldser, D., Huarte, M., Zuk, O., Carey, B.W., Cassady, J.P., et al. (2009). Chromatin signature reveals over a thousand highly conserved large non-coding RNAs in mammals. Nature *458*, 223–227. https://doi.org/10.1038/nature07672.

6. Mercer, T.R., Dinger, M.E., Sunkin, S.M., Mehler, M.F., and Mattick, J.S. (2008). Specific expression of long noncoding RNAs in the mouse brain. Proc. Natl. Acad. Sci. USA *105*, 716–721. https://doi.org/10.1073/pnas.0706729105.

7. Ravasi, T., Suzuki, H., Pang, K.C., Katayama, S., Furuno, M., Okunishi, R., Fukuda, S., Ru, K., Frith, M.C., Gongora, M.M., et al. (2006). Experimental validation of the regulated expression of large numbers of non-coding RNAs from the mouse genome. Genome Res. *16*, 11–19. https://doi.org/10.1101/gr.4200206.

8. Ghanam, A.R., Cao, J., Ouyang, X., and Song, X. (2019). New insights into chronological mobility of retrotransposons in vivo. Oxid. Med. Cell. Longev. *2019*, 2818415. https://doi.org/10.1155/2019/2818415.

9. Ghanam, A.R., Xu, Q., Ke, S., Azhar, M., Cheng, Q., and Song, X. (2017). Shining the light on senescence associated LncRNAs. Aging Dis. *8*, 149–161. https://doi.org/10.14336/ad.2016.0810.

10. Hutchinson, J.N., Ensminger, A.W., Clemson, C.M., Lynch, C.R., Lawrence, J.B., and Chess, A. (2007). A screen for nuclear transcripts identifies two linked noncoding RNAs associated with SC35 splicing domains. BMC Genom. *8*, 39. https://doi.org/10.1186/1471-2164-8-39.

11. Wilusz, J.E., Freier, S.M., and Spector, D.L. (2008). 3′ end processing of a long nuclear-retained noncoding RNA yields a tRNA-like cytoplasmic RNA. Cell *135*, 919–932. https://doi.org/10.1016/j.cell.2008.10.012.

12. Gutschner, T., Hämmerle, M., and Diederichs, S. (2013). MALAT1 – a paradigm for long noncoding RNA function in cancer. J. Mol. Med. *91*, 791–801. https://doi.org/10.1007/s00109-013-1028-y.

13. West, J.A., Davis, C.P., Sunwoo, H., Simon, M.D., Sadreyev, R.I., Wang, P.I., Tolstorukov, M.Y., and Kingston, R.E. (2014). The long noncoding RNAs NEAT1 and MALAT1 bind active chromatin sites. Mol. Cell *55*, 791–802. https://doi.org/10.1016/j.molcel.2014.07.012.

14. Zhang, B., Arun, G., Mao, Y.S., Lazar, Z., Hung, G., Bhattacharjee, G., Xiao, X., Booth, C.J., Wu, J., Zhang, C., and Spector, D.L. (2012). The lncRNA Malat1 is dispensable for mouse development but its transcription plays a cis-regulatory role in the adult. Cell Rep. *2*, 111–123. https://doi.org/10.1016/j.celrep.2012.06.003.

15. Nakagawa, S., Ip, J.Y., Shioi, G., Tripathi, V., Zong, X., Hirose, T., and Prasanth, K.V. (2012). Malat1 is not an essential component of nuclear speckles in mice. RNA *18*, 1487–1499. https://doi.org/10.1261/rna.033217.112.

16. Eißmann, M., Gutschner, T., Hämmerle, M., Günther, S., Caudron-Herger, M., Groß, M., Schirmacher, P., Rippe, K., Braun, T., Zörnig, M., and Diederichs, S. (2012). Loss of the abundant nuclear non-coding RNA MALAT1 is compatible with life and development. RNA Biol. *9*, 1076–1087. https://doi.org/10.4161/rna.21089.

17. Yao, J., Wang, X.Q., Li, Y.J., Shan, K., Yang, H., Wang, Y.N.Z., Yao, M.D., Liu, C., Li, X.M., Shen, Y., et al. (2016). Long non-coding RNA MALAT1 regulates retinal neurodegeneration through CREB signaling. EMBO Mol. Med. *8*, 1113. https://doi.org/10.15252/emmm.201606749.

18. Bernard, D., Prasanth, K.V., Tripathi, V., Colasse, S., Nakamura, T., Xuan, Z., Zhang,

M.Q., Sedel, F., Jourdren, L., Coulpier, F., et al. (2010). A long nuclear-retained non-coding RNA regulates synaptogenesis by modulating gene expression. EMBO J. *29*, 3082–3093. https://doi.org/10.1038/emboj.2010.199.

19. Dreos, R., Ambrosini, G., Groux, R., Cavin Périer, R., and Bucher, P. (2017). The eukaryotic promoter database in its 30th year: focus on non-vertebrate organisms. Nucleic Acids Res. *45*, D51–D55. https://doi.org/10.1093/nar/gkw1069.

20. Suzuki, A., Kawano, S., Mitsuyama, T., Suyama, M., Kanai, Y., Shirahige, K., Sasaki, H., Tokunaga, K., Tsuchihara, K., Sugano, S., et al. (2018). DBTSS/DBKERO for integrated analysis of transcriptional regulation. Nucleic Acids Res. *46*, D229–D238. https://doi.org/10.1093/nar/gkx1001.

21. Cabili, M.N., Trapnell, C., Goff, L., Koziol, M., Tazon-Vega, B., Regev, A., and Rinn, J.L. (2011). Integrative annotation of human large intergenic noncoding RNAs reveals global properties and specific subclasses. Genes Dev. *25*, 1915–1927. https://doi.org/10.1101/gad.17446611.

22. Ma, X.Y., Wang, J.H., Wang, J.L., Ma, C.X., Wang, X.C., and Liu, F.S. (2015). Malat1 as an evolutionarily conserved lncRNA, plays a positive role in proliferation and maintaining undifferentiated status of early-stage hematopoietic cells. BMC Genom. *16*, 676. https://doi.org/10.1186/s12864-015-1881-x.

23. Delli Ponti, R., Armaos, A., Marti, S., and Tartaglia, G.G. (2018). A method for RNA structure prediction shows evidence for structure in lncRNAs. Front. Mol. Biosci. *5*, 111. https://doi.org/10.3389/fmolb.2018.00111.

24. D'Aquila, P., Montesanto, A., Mandalà, M., Garasto, S., Mari, V., Corsonello, A., Bellizzi, D., and Passarino, G. (2017). Methylation of the ribosomal RNA gene promoter is associated with aging and age-related decline. Aging Cell *16*, 966–975. https://doi.org/10.1111/acel.12603.

25. Rizvi, S., Raza, S.T., and Mahdi, F. (2014). Telomere length variations in aging and age-related diseases. Curr. Aging Sci. *7*, 161–167. https://doi.org/10.2174/1874609808666150122153151.

26. Chen, R., Liu, Y., Zhuang, H., Yang, B., Hei, K., Xiao, M., Hou, C., Gao, H., Zhang, X., Jia, C., et al. (2017). Quantitative proteomics reveals that long non-coding RNA MALAT1 interacts with DBC1 to regulate p53 acetylation. Nucleic Acids Res. *45*, 9947–9959. https://doi.org/10.1093/nar/gkx600.

27. Yang, F., Yi, F., Han, X., Du, Q., and Liang, Z. (2013). MALAT-1 interacts with hnRNP C in cell cycle regulation. FEBS Lett. *587*, 3175–3181. https://doi.org/10.1016/j.febslet.2013.07.048.

28. Chen, X., He, L., Zhao, Y., Li, Y., Zhang, S., Sun, K., So, K., Chen, F., Zhou, L., Lu, L., et al. (2017). Malat1 regulates myogenic differentiation and muscle regeneration through modulating MyoD transcriptional activity. Cell Discov. *3*, 17002. https://doi.org/10.1038/celldisc.2017.2.

29. Singh, K., Cassano, M., Planet, E., Sebastian, S., Jang, S.M., Sohi, G., Faralli, H., Choi, J., Youn, H.D., Dilworth, F.J., and Trono, D. (2015). A KAP1 phosphorylation switch controls MyoD function during skeletal muscle differentiation. Genes Dev. *29*, 513–525. https://doi.org/10.1101/gad.254532.114.

30. Santos, J., and Gil, J. (2014). TRIM28/KAP1 regulates senescence. Immunol. Lett. *162*, 281–289. https://doi.org/10.1016/j.imlet.2014.08.011.

31. Lee, H., Arnouk, H., Sripathi, S., Chen, P., Zhang, R., Bartoli, M., Hunt, R.C., Hrushesky, W.J.M., Chung, H., Lee, S.H., and Jahng, W.J. (2010). Prohibitin as an oxidative stress biomarker in the eye. Int. J. Biol. Macromol. *47*, 685–690. https://doi.org/10.1016/j.ijbiomac.2010.08.018.

32. Schaefer, U., Kodzius, R., Kai, C., Kawai, J., Carninci, P., Hayashizaki, Y., and Bajic, V.B. (2010). High sensitivity TSS prediction: estimates of locations where TSS cannot occur. PLoS One 5, e13934. https://doi.org/10.1371/journal.pone.0013934.

33. Metsalu, T., and Vilo, J. (2015). ClustVis: a web tool for visualizing clustering of multivariate data using Principal Component Analysis and heatmap. Nucleic Acids Res. *43*, W566–W570. https://doi.org/10.1093/nar/gkv468.

34. Johnson, I.P. (2015). Age-related neurodegenerative disease research needs aging models. Front. Aging Neurosci. *7*, 168. https://doi.org/10.3389/fnagi.2015.00168.

35. Baker, M.L., Hand, P.J., Wang, J.J., and Wong, T.Y. (2008). Retinal signs and stroke: revisiting the link between the eye and brain. Stroke *39*, 1371–1379. https://doi.org/10.1161/strokeaha.107.496091.

36. Gan, L., and Mucke, L. (2008). Paths of convergence: sirtuins in aging and neurodegeneration. Neuron *58*, 10–14. https://doi.org/10.1016/j.neuron.2008.03.015.

37. Oberdoerffer, P., Michan, S., McVay, M., Mostoslavsky, R., Vann, J., Park, S.K., Hartlerode, A., Stegmuller, J., Hafner, A., Loerch, P., et al. (2008). SIRT1 redistribution on chromatin promotes genomic stability but alters gene expression during aging. Cell *135*, 907–918. https://doi.org/10.1016/j.cell.2008.10.025.

38. den Haan, J., Janssen, S.F., van de Kreeke, J.A., Scheltens, P., Verbraak, F.D., and Bouwman, F.H. (2018). Retinal thickness correlates with parietal cortical atrophy in early-onset Alzheimer's disease and controls. Alzheimers Dement. *10*, 49–55. https://doi.org/10.1016/j.dadm.2017.10.005.

39. Yu, J.G., Feng, Y.F., Xiang, Y., Huang, J.H., Savini, G., Parisi, V., Yang, W.J., and Fu, X.A. (2014). Retinal nerve fiber layer thickness changes in Parkinson disease: a meta-analysis. PLoS One 9, e85718. https://doi.org/10.1371/journal.pone.0085718.

40. Thomson, K.L., Yeo, J.M., Waddell, B., Cameron, J.R., and Pal, S. (2015). A systematic review and meta-analysis of retinal nerve fiber layer change in dementia, using optical coherence tomography. Alzheimers Dement. *1*, 136–143. https://doi.org/10.1016/j.dadm.2015.03.001.

41. Liu, S., Ong, Y.T., Hilal, S., Loke, Y.M., Wong, T.Y., Chen, C.L.H., Cheung, C.Y., and Zhou, J. (2016). The association between retinal neuronal layer and brain structure is disrupted in patients with cognitive impairment and Alzheimer's disease. J. Alzheimers Dis. *54*, 585–595. https://doi.org/10.3233/jad-160067.

42. Casaletto, K.B., Ward, M.E., Baker, N.S., Bettcher, B.M., Gelfand, J.M., Li, Y., Chen, R., Dutt, S., Miller, B., Kramer, J.H., and Green, A.J. (2017). Retinal thinning is uniquely associated with medial temporal lobe atrophy in neurologically normal older adults. Neurobiol. Aging *51*, 141–147. https://doi.org/10.1016/j.neurobiolaging.2016.12.011.

43. Jorge, L., Canário, N., Quental, H., Bernardes, R., and Castelo-Branco, M. (2019). Is the retina a mirror of the aging brain? Aging of neural retina layers and primary visual cortex across the lifespan. Front. Aging Neurosci. *11*, 360. https://doi.org/10.3389/fnagi.2019.00360.

44. Hosokawa, M., Takeshita, S., Higuchi, K., Shimizu, K., Irino, M., Toda, K., Honma, A., Matsumura, A., Yasuhira, K., and Takeda, T. (1984). Cataract and other ophthalmic lesions in senescence accelerated mouse (SAM). Morphology and incidence of senescence associated ophthalmic changes in mice. Exp. Eye Res. *38*, 105–114. https://doi.org/10.1016/0014-4835(84)90095-2.

45. Hosokawa, M., Umezawa, M., Higuchi, K., and Takeda, T. (1998). Interventions of senescence in SAM mice. J. Anti Aging Med. *1*, 27–37. https://doi.org/10.1089/rej.1998.1.27.

46. Cejka, C., and Cejkova, J. (2015). Oxidative stress to the cornea, changes in corneal optical properties, and advances in treatment of corneal oxidative injuries. Oxid. Med. Cell. Longev. *2015*, 591530. https://doi.org/10.1155/2015/591530.

47. Alves, C., Batista, S., d'Almeida, O.C., Sousa, L., Cunha, L., Bernardes, R., and Castelo-Branco, M. (2018). The retinal ganglion cell layer predicts normal-appearing white matter tract integrity in multiple sclerosis: a combined diffusion tensor imaging and optical coherence tomography approach. Hum. Brain Mapp. *39*, 1712–1720. https://doi.org/10.1002/hbm.23946.

48. Grzybowski, A., and Barboni, P. (2016). Introduction: retina imaging–past and present. In OCT in Central Nervous System Diseases (Springer), pp. 1–5.

49. Drummond-Barbosa, D. (2008). Stem cells, their niches and the systemic environment: an aging network. Genetics *180*, 1787–1797. https://doi.org/10.1534/genetics.108.098244.

50. Baker, D.J., Childs, B.G., Durik, M., Wijers, M.E., Sieben, C.J., Zhong, J., Saltness, R.A., Jeganathan, K.B., Verzosa, G.C., Pezeshki, A., et al. (2016). Naturally occurring p16(Ink4a)-positive cells shorten healthy lifespan. Nature *530*, 184–189. https://doi.org/10.1038/nature16932.

51. Liu, B., and Zhou, Z. (2013). Activation of SIRT1 by resveratrol requires lamin A. Aging *5*, 94–95. https://doi.org/10.18632/aging.100532.

52. Johansson, H., and Simonsson, S. (2010). Core transcription factors, Oct4, Sox2 and Nanog, individually form complexes with nucleophosmin (Npm1) to control embryonic stem (ES) cell fate determination. Aging *2*, 815–822. https://doi.org/10.18632/aging.100222.

53. Cimadamore, F., Amador-Arjona, A., Chen, C., Huang, C.T., and Terskikh, A.V. (2013). SOX2-LIN28/let-7 pathway regulates proliferation and neurogenesis in neural precursors. Proc. Natl. Acad. Sci. USA *110*, E3017–E3026. https://doi.org/10.1073/pnas.1220176110.

54. Macleod, K.F., Sherry, N., Hannon, G., Beach, D., Tokino, T., Kinzler, K., Vogelstein, B., and Jacks, T. (1995). p53-dependent and independent expression of p21 during cell growth, differentiation, and DNA damage. Genes Dev. *9*, 935–944. https://doi.org/10.1101/gad.9.8.935.

55. Xiao, J., Zhang, Z., Chen, G.G., Zhang, M., Ding, Y., Fu, J., Li, M., and Yun, J.P. (2009). Nucleophosmin/B23 interacts with p21WAF1/CIP1 and contributes to its stability. Cell Cycle *8*, 889–895. https://doi.org/10.4161/cc.8.6.7898.

56. Fukuchi, K., Maruyama, H., Takagi, Y., and Gomi, K. (1999). Direct proteasome inhibition by clasto-lactacystin beta-lactone permits the detection of ubiquitinated p21(waf1) in ML-1 cells. Biochim. Biophys. Acta *1451*, 206–210. https://doi.org/10.1016/s0167-4889(99)00081-6.

57. Blagosklonny, M.V., Wu, G.S., Omura, S., and el-Deiry, W.S. (1996). Proteasome-dependent regulation of p21WAF1/CIP1 expression. Biochem. Biophys. Res. Commun. *227*, 564–569. https://doi.org/10.1006/bbrc.1996.1546.

58. Maki, C.G., and Howley, P.M. (1997). Ubiquitination of p53 and p21 is differentially affected by ionizing and UV radiation. Mol. Cell Biol. *17*, 355–363. https://doi.org/10.1128/mcb.17.1.355.

59. Vasquez, K.M., Marburger, K., Intody, Z., and Wilson, J.H. (2001). Manipulating the mammalian genome by homologous recombination. Proc. Natl. Acad. Sci. USA *98*, 8403–8410. https://doi.org/10.1073/pnas.111009698.

60. Yamane-Ohnuki, N., Kinoshita, S., Inoue-Urakubo, M., Kusunoki, M., Iida, S., Nakano, R., Wakitani, M., Niwa, R., Sakurada, M., Uchida, K., et al. (2004). Establishment of FUT8 knockout Chinese hamster ovary cells: an ideal host cell line for producing completely defucosylated antibodies with enhanced antibody-dependent cellular cytotoxicity. Biotechnol. Bioeng. *87*, 614–622. https://doi.org/10.1002/bit.20151.

61. Sunwoo, J.S., Lee, S.T., Im, W., Lee, M., Byun, J.I., Jung, K.H., Park, K.I., Jung, K.Y., Lee, S.K., Chu, K., and Kim, M. (2017). Altered expression of the long noncoding RNA NEAT1 in Huntington's disease. Mol. Neurobiol. *54*, 1577–1586. https://doi.org/10.1007/s12035-016-9928-9.

62. Cremer, S., Michalik, K.M., Fischer, A., Pfisterer, L., Jaé, N., Winter, C., Boon, R.A., Muhly-Reinholz, M., John, D., Uchida, S., et al. (2019). Hematopoietic deficiency of the long noncoding RNA MALAT1 promotes atherosclerosis and plaque inflammation. Circulation *139*, 1320–1334. https://doi.org/10.1161/circulationaha.117.029015.

63. Michalik, K.M., You, X., Manavski, Y., Doddaballapur, A., Zörnig, M., Braun, T., John, D., Ponomareva, Y., Chen, W., Uchida, S., et al. (2014). Long noncoding RNA MALAT1 regulates endothelial cell function and vessel growth. Circ. Res. *114*, 1389–1397. https://doi.org/10.1161/circresaha.114.303265.

64. Shoji, M., Okada, M., Ohta, A., Higuchi, K., Hosokawa, M., and Honda, Y. (1998). A morphological and morphometrical study of the retina in aging SAM mice. Ophthalmic Res. *30*, 172–179. https://doi.org/10.1159/000055471.

65. Takeda, T., Hosokawa, M., Higuchi, K., Hosono, M., Akiguchi, I., and Katoh, H. (1994). A novel murine model of aging, Senescence-Accelerated Mouse (SAM). Arch. Gerontol. Geriatr. *19*, 185–192. https://doi.org/10.1016/0167-4943(94)90039-6.

66. Hosokawa, M., and Ueno, M. (1999). Aging of blood-brain barrier and neuronal cells of eye and ear in SAM mice. Neurobiol. Aging *20*, 117–123. https://doi.org/10.1016/s0197-4580(99)00029-9.

67. Madelaine, R., and Mourrain, P. (2017). Endogenous retinal neural stem cell reprogramming for neuronal regeneration. Neural Regen. Res. *12*, 1765–1767. https://doi.org/10.4103/1673-5374.219028.

68. Evans, D.S., Kapahi, P., Hsueh, W.C., and Kockel, L. (2011). TOR signaling never gets old: aging, longevity and TORC1 activity. Ageing Res. Rev. *10*, 225–237. https://doi.org/10.1016/j.arr.2010.04.001.

69. Bemiller, P.M., and Lee, L.H. (1978). Nucleolar changes in senescing WI-38 cells. Mech. Ageing Dev. *8*, 417–427. https://doi.org/10.1016/0047-6374(78)90041-6.

70. Buchwalter, A., and Hetzer, M.W. (2017). Nucleolar expansion and elevated protein translation in premature aging. Nat. Commun. *8*, 328. https://doi.org/10.1038/s41467-017-00322-z.

71. Hansen, M., Taubert, S., Crawford, D., Libina, N., Lee, S.J., and Kenyon, C. (2007). Lifespan extension by conditions that inhibit translation in Caenorhabditis elegans. Aging Cell *6*, 95–110. https://doi.org/10.1111/j.1474-9726.2006.00267.x.

72. Syntichaki, P., Troulinaki, K., and Tavernarakis, N. (2007). eIF4E function in somatic cells modulates ageing in Caenorhabditis elegans. Nature *445*, 922–926. https://doi.org/10.1038/nature05603.

73. Murayama, A., Ohmori, K., Fujimura, A., Minami, H., Yasuzawa-Tanaka, K., Kuroda, T., Oie, S., Daitoku, H., Okuwaki, M., Nagata, K., et al. (2008). Epigenetic control of rDNA loci in response to intracellular energy status. Cell *133*, 627–639. https://doi.org/10.1016/j.cell.2008.03.030.

74. Tiku, V., Jain, C., Raz, Y., Nakamura, S., Heestand, B., Liu, W., Späth, M., Suchiman, H.E.D., Müller, R.U., Slagboom, P.E., et al. (2017). Small nucleoli are a cellular hallmark of longevity. Nat. Commun. *8*, 16083. https://doi.org/10.1038/ncomms16083.

75. Savkur, R.S., and Olson, M.O. (1998). Preferential cleavage in pre-ribosomal RNA byprotein B23 endoribonuclease. Nucleic Acids Res. *26*, 4508–4515. https://doi.org/10.1093/nar/26.19.4508.

76. Murano, K., Okuwaki, M., Hisaoka, M., and Nagata, K. (2008). Transcription regulation of the rRNA gene by a multifunctional nucleolar protein, B23/nucleophosmin, through its histone chaperone activity. Mol. Cell Biol. *28*, 3114–3126. https://doi.org/10.1128/mcb.02078-07.

77. Safaiyan, S., Kannaiyan, N., Snaidero, N., Brioschi, S., Biber, K., Yona, S., Edinger, A.L., Jung, S., Rossner, M.J., and Simons, M. (2016). Age-related myelin degradation burdens the clearance function of microglia during aging. Nat. Neurosci. *19*, 995–998. https://doi.org/10.1038/nn.4325.

78. Bolger, A.M., Lohse, M., and Usadel, B. (2014). Trimmomatic: a flexible trimmer for Illumina sequence data. Bioinformatics *30*, 2114–2120. https://doi.org/10.1093/bioinformatics/btu170.

79. Dobin, A., Davis, C.A., Schlesinger, F., Drenkow, J., Zaleski, C., Jha, S., Batut, P., Chaisson, M., and Gingeras, T.R. (2013). STAR: ultrafast universal RNA-seq aligner. Bioinformatics *29*, 15–21. https://doi.org/10.1093/bioinformatics/bts635.

80. Love, M.I., Huber, W., and Anders, S. (2014). Moderated estimation of fold change and dispersion for RNA-seq data with DESeq2. Genome Biol. *15*, 550. https://doi.org/10.1186/s13059-014-0550-8.

81. Xie, C., Mao, X., Huang, J., Ding, Y., Wu, J., Dong, S., Kong, L., Gao, G., Li, C.Y., and Wei, L. (2011). Kobas 2.0: a web server for annotation and identification of enriched pathways and diseases. Nucleic Acids Res. *39*, W316–W322. https://doi.org/10.1093/nar/gkr483.

82. Subramanian, A., Tamayo, P., Mootha, V.K., Mukherjee, S., Ebert, B.L., Gillette, M.A., Paulovich, A., Pomeroy, S.L., Golub, T.R., Lander, E.S., and Mesirov, J.P. (2005). Gene set enrichment analysis: a knowledge-based approach for interpreting genome-wide expression profiles. Proc. Natl. Acad. Sci. USA

102, 15545–15550. https://doi.org/10.1073/pnas.0506580102.

83. Bartkova, J., Rezaei, N., Liontos, M., Karakaidos, P., Kletsas, D., Issaeva, N., Vassiliou, L.V.F., Kolettas, E., Niforou, K., Zoumpourlis, V.C., et al. (2006). Oncogene-induced senescence is part of the tumorigenesis barrier imposed by DNA damage checkpoints. Nature *444*, 633–637. https://doi.org/10.1038/nature05268.

84. Liu, C., Xie, W., Gui, C., and Du, Y. (2013). Pronuclear microinjection and oviduct transfer procedures for transgenic mouse production. Methods Mol. Biol. *1027*, 217–232. https://doi.org/10.1007/978-1-60327-369-5_10.

85. Claybon, A., and Bishop, A.J. (2011). Dissection of a mouse eye for a whole mount of the retinal pigment epithelium. J. Vis. Exp. *48*, 2563. https://doi.org/10.3791/2563.

86. Chu, C., Quinn, J., and Chang, H.Y. (2012). Chromatin isolation by RNA purification (ChIRP). J. Vis. Exp. *61*, 3912. https://doi.org/10.3791/3912.

87. Wiśniewski, J.R., Zougman, A., Nagaraj, N., and Mann, M. (2009). Universal sample preparation method for proteome analysis. Nat. Methods *6*, 359–362. https://doi.org/10.1038/nmeth.1322.

88. Choo, Y.S., and Zhang, Z. (2009). Detection of protein ubiquitination. J. Vis. Exp. *30*, 1293. https://doi.org/10.3791/1293.

89. Yang, W.S., Campbell, M., Kung, H.J., and Chang, P.C. (2018). In vitro SUMOylation assay to study SUMO E3 ligase activity. J. Vis. Exp. *131*, 56629. https://doi.org/10.3791/56629.

90. Gaspar, I., Wippich, F., and Ephrussi, A. (2017). Enzymatic production of single-molecule FISH and RNA capture probes. RNA *23*, 1582–1591. https://doi.org/10.1261/rna.061184.117.

91. Gagliardi, M., and Matarazzo, M.R. (2016). RIP: RNA immunoprecipitation. Methods Mol. Biol. *1480*, 73–86. https://doi.org/10.1007/978-1-4939-6380-5_7.

92. Ratnadiwakara, M., and Änkö, M.L. (2018). mRNA stability assay using transcription inhibition by Actinomycin D in mouse pluripotent stem cells. Bio. Protoc. *8*, e3072. https://doi.org/10.21769/BioProtoc.3072.

93. Chan, T.F., Chiu, K., Lok, C.K., Lau, H.W., So, K.F., and Chang, R.C. (2012). Morphometric analyses of retinal sections. J. Vis. Exp. *60*, 3377. https://doi.org/10.3791/3377.

94. Putri, G.H., Anders, S., Pyl, P.T., Pimanda, J.E., and Zanini, F. (2022). Analysing high-throughput sequencing data in Python with HTSeq 2.0. Bioinformatics *38*, 2943–2945. https://doi.org/10.1093/bioinformatics/btac166.

95. Labun, K., Montague, T.G., Krause, M., Torres Cleuren, Y.N., Tjeldnes, H., and Valen, E. (2019). CHOPCHOP v3: expanding the CRISPR web toolbox beyond genome editing. Nucleic Acids Res. *47*, W171–W174. https://doi.org/10.1093/nar/gkz365.

96. Concordet, J.-P., and Haeussler, M. (2018). CRISPOR: intuitive guide selection for CRISPR/Cas9 genome editing experiments and screens. Nucleic Acids Res. *46*, W242–W245. https://doi.org/10.1093/nar/gky354.

STAR★METHODS

KEY RESOURCES TABLE

REAGENT or RESOURCE	SOURCE	IDENTIFIER
Antibodies		
KAP1 Antibody	Proteintech	Cat #15202-1-AP; RRID:AB_2209890
p53 Antibody	SantaCruz	Cat #SC-126; RRID:AB_628082
p21 Antibody	Millipore	Cat #05-345; RRID:AB_309684
PHB1 Antibody	CST	Cat #2426; RRID:AB_823689
PHB2 (E1Z5A) Antibody	CST	Cat #14085; RRID:AB_2798387
B23/NPM1 Antibody	Proteintech	Cat #60096-1-Ig; RRID:AB_2155162
hnRNP C1/C2 Antibody	SantaCruz	Cat #sc-32308; RRID:AB_627731
TRIM29 Antibody	Proteintech	Cat #17542-1-AP; RRID:AB_2272412
LIN28 Antibody	Proteintech	Cat #11724-1-AP; RRID:AB_2135039
SUMO2/3 Antibody	Proteintech	Cat #11251-1-AP; RRID:AB_2198405
hnRNP C1 + C2 Antibody	Abcam	Cat #ab128049; RRID:AB_11141461
hnRNPC Antibody	Proteintech	Cat #11760-1-AP; RRID:AB_2117500
GAPDH Antibody	Proteintech	Cat #60004-1-Ig; RRID:AB_2107436
Beta Tubulin antibody	Proteintech	Cat #66240-1-Ig; RRID:AB_2881629
Uiqutin Antibody	SantaCruz	Cat #sc-8017; RRID:AB_628423
HRP-Goat Anti-Mouse IgG	Proteintech	Cat #SA00002-1; RRID:AB_2890887
HRP-Goat Anti-Rabbit IgG	Proteintech	Cat #SA00001-2; RRID:AB_2722564
Normal rabbit IgG	CST	Cat #27795
Biotin Antibody	Abcam	Cat #ab201341
Alexa Fluor® 488	Proteintech	Cat #Alexa Flour 488
Chemicals, peptides, and recombinant proteins		
Sodium chloride (NaCl)	Sigma Aldrich	Cat # S3014
Trizma base	Sigma Aldrich	Cat #77-86-1
EDTA	Sigma Aldrich	Cat # E5134
PMSF	Roche	Cat #1837091001
Protease inhibitors	Roche	Cat #4906837001
Sodium Deoxycholate	Sigma Aldrich	Cat #302-95-4
Sodium dodecyl sulfate	Sigma Aldrich	Cat #151-21-3
NP-40	Thermo Scientific	Cat #85124
HEPES	Invitrogen	Cat #15630080
MgCl2	Invitrogen	Cat #AM9530G
PVDF- membranes	Millipore	Cat # IPVH00010
BSA blocking buffer	Sangon Biotech	Cat #9048-46-8
TBST	CWBIO	Cat #CW0043S
ECL-Western blot kits	Advansta	Cat # K-12045-D10
TRIzol Reagent	Invitrogen®	Cat #15596018
TRizol LS	Invitrogen®	Cat #10296-028
Yeast tRNA	Invitrogen	Cat #AM7119
Formamide	Sigma	Cat #75-12-7
Vanadyl Ribonucleoside Complex	Sigma	Cat #R3380-5ML
Dextran Sulfate	Sigma	Cat #42867

(Continued on next page)

Continued

REAGENT or RESOURCE	SOURCE	IDENTIFIER
RNase-free BSA	Sangon Biotech	Cat # 9048-46-8
RNase-Free DNase	Promega	Cat #M6101
RNase inhibitor	Promega	Cat #N2615
Protein A/G magnetic beads	Thermo Scientific	Cat #88803
T7 Endonuclease I	NEB	Cat #M0302L
Deposited data		
Raw and analyzed data	This paper	GSE130392
Experimental models: Cell lines		
HEK293T	Thermo Fisher Scientific	
Neuro-2a (N2A)	Dr Jiangning Zhou (USTC), ATCC	Cat #CCL-131; RRID:CVCL_0470
NIH-3T3	ATCC	Cat # CRL-1658; RRID:CVCL_0594
DMEM medium	Invitrogen®	Cat #12800017
Fetal Bovine Serum (FBS)	Invitrogen®	Cat #1009941.0
L-glutamine	Wisent®	Cat #609-065-EL
Penicillin–Streptomycin	Wisent®	Cat #40-201-EL
Lipofectamine 2000	Invitrogen®	Cat #116681019
Opti-MEMI	Invitrogen®	Cat #31985070
C57BL/6 mice	Wild type	Vital River Laboratories (Beijing, China)
*Malat1*Δ1 mice	This study	
*Malat1*Δ2 mice	This study	
Experimental models: Organisms/strains		
C57BL/6 mice	Wild type	Vital River Laboratories (Beijing, China)
*Malat1*Δ1 mice	This study	
*Malat1*Δ2 mice	This study	
Oligonucleotides		
Primers for qRT-PCR	This paper	N/A
shRNAs oligonucleotides	This paper	N/A
sgRNAs and PCR genotyping primers	This paper	N/A
Malat1 biotin labeled probes	This paper	N/A
Lac Z biotin labeled probes	This paper	N/A
Recombinant DNA		
NLS-flag-linker-Cas9	Addgene	Cat #44758; RRID:Addgene_44758
Puc57-sgRNA	Addgene	Cat #51132; RRID:Addgene_51132
Critical commercial assays		
mMESSAGE mMACHINE® T7 Ultra Kit	Ambion	Cat #AM1345
MEGAshortscript™ Kit	Ambion	Cat #AM1354
Software and algorithms		
CRISPOR	Concordet et al. (2018)[96]	http://crispor.tefor.net
ChopChop	Labun et al. (2019)[95]	https://chopchop.rc.fas.harvard.edu
Image J program	NIH	imagej.nih.gov/ij/download/
FastQC v.0.11.4		http://www.bioinformatics.babraham.ac.uk/projects/fastqc
Trimmomatic	Bolger et al (2014)[78]	http://www.usadellab.org/cms/index.php?page=trimmomatic
STAR v.2.7	Dobin et al. (2012)[79]	https://code.google.com/archive/p/rna-star/
HTSeq v.0.6.1	Putri et al. (2021)[94]	https://htseq.readthedocs.io/en/master/

Continued

REAGENT or RESOURCE	SOURCE	IDENTIFIER
R package v.1.22.2	Love (2014)[80]	http://www.bioconductor.org/packages/release/bioc/html/DESeq2.html
KOBAS 3 database	Xie et al. (2011)[81]	http://kobas.cbi.pku.edu.cn
GSEA v.4.0	Subramanian et al. (2015)[82]	http://www.gsea-msigdb.org/gsea/index.jsp

RESOURCE AVAILABILITY

Lead contact

Further information and requests for resources and reagents should be directed to and will be fulfilled by the lead contact, Xiaoyuan Song (songxy5@ustc.edu.cn).

Materials availability

This study did not generate new unique reagents.

Data and code availability

This paper analyzed the total RNAs that were extracted from *Malat1* wild type (WT), *Malat1*Δ1, and *Malat1*Δ2 brain tissues (two duplicates per group) using TRIzol Reagent. RNase-Free DNase was used to eliminate DNA contamination. A minimum of 2 μg RNA was subjected to mRNAs and lncRNAs sequencing (Ribo-minus RNA-seq) at the Neogene Sequencing and Microarray Core Facility. The raw 150 bp paired-end sequences (Sanger/Illumina 1.9 encoding) were quality controlled using FastQC v.0.11.4 (http://www.bioinformatics.babraham.ac.uk/projects/fastqc/), and the low-quality bases (quality scores <30) and adaptor contamination (if present) were removed by Trimmomatic v.0.36 81. The high-quality reads were mapped by STAR v.2.7 82 against the *Mus musculus* mm10 primary assembly genome. The uniquely-mapped reads aligned to exons were counted with HTSeq v.0.6.1,[83] then tested for the presence of differentially expressed genes (DE-Gs) by the DESeq2 R package v.1.22.284. All genes with false discovery rate (FDR)-adjusted P-values less than 0.1 were considered DEGs regardless of their fold-change (FC) value. Functional analysis of the DEGs was performed using enrichment analysis for specific Gene Ontology (GO) terms using the KOBAS 3 database 85. Gene set enrichment analysis (GSEA) was conducted using GSEA software version 4.086. The sequencing data (FASTQ files) associated with this project are deposited in the Gene Expression Omnibus (GEO) under the accession number GSE130392.

EXPERIMENTAL MODEL AND SUBJECT DETAILS

Ethics committees statement

All the experimental procedure on mice was approved by the University of Science and Technology of China (USTC) Animal Resources Center and University Animal Care and Use Committee and the protocol was approved by the Committee on the Ethics of Animal Experiments of the USTC (Permit Number: PXHG-SXY201510183). Young (1 month) and aged (20 months) old mice of both sex were euthanized with 8% chloral hydrate followed by cervical dislocation and organs were dissected in cold 1X PBS then used either for RNA or protein extraction.

Mouse models

To generate *Malat1*Δ1, and *Malat1*Δ2mice with targeted disruption of *Malat1*, sgRNA were designed from crispr.mit.edu. sgRNA and PCR genotyping primers were listed (Table S8), followed by cloning in Bsa1 digested sgRNA expression vector. Clones were verified for right insertion through Sanger sequencing, sgRNA plasmids were co-transfected with the WT-Cas9 expression vector (Addgene #44758) as previously described. 72 h post transfection mismatching efficiency was determined by T7E1 (NEB, M0302L) according to the manufacturer protocol. For clonal expansion, cells were plated in 96-well plates using limited dilution methods and grown for one to two weeks. Isolated clones were subjected to genotyping by PCR followed by DNA sequencing and RT-qPCR for knockout validation. *In vitro* verified sgRNAs were cloned into Bsa1 linearized Puc57-sgRNA (Addgene #51132), correct insertion was verified by Sanger sequencing, then sgRNA were *in vitro*-transcribed using MEGAshortscript™ Kit (Ambion, #AM1354) according to the manufacturer's instructions. pST1374-NLS-flag-linker-Cas9 (Addgene #44758) was *in vitro*-transcribed using mMESSAGE mMACHINE® T7 Ultra Kit (Ambion, #AM1345), purified sgRNA and

pST1374-NLS-flag-linker-Cas9 mRNA (addgene #44758) were microinjected into mouse embryos as described previously.[84] The offspring were genotyped and the primer sequences for PCR genotyping were listed in (Table S8). The purity of all mouse strains used in this study was greater than 98%.

METHODS DETAILS

Cell culture and transfection

The HEK293T cell line was from Thermo Fisher Scientific. Neuro-2a (N2A) and NIH3T3 cells were obtained from the American Type Culture Collection (ATCC). The cells were cultured in DMEM medium (Invitrogen® #12800017) supplemented with 10% FBS (Invitrogen® #1009941.0), 4mM L-glutamine (Wisent® #609-065-EL), and 1:100 penicillin–streptomycin (Wisent® #40-201-EL) at 37°C in a 5% CO2 incubator. Lipofectamine 2000 (Invitrogen® #116681019) and Opti-MEM I (Invitrogen® #31985070) were used for transient transfection according to the manufacturer's protocol.

Immunoblotting and western blot

All steps were performed according to the manufacturer's protocol, using a Bio-Rad system (Bio-Rad, USA). Briefly, fresh brains were cut into small pieces using scissors and then homogenized in RIPA lysis buffer (150 mM NaCl; 1.0% NP40; 0.5% sodium deoxycholate; 0.1% SDS; 50 mM Tris-HCl, pH 8.0) with protease inhibitors. The homogenized samples were slowly rotated at 4°C for 2 h followed by sonication for 5 min, followed by centrifugation at 12,000 g at 4 °C for 10 min. After that, the supernatant was collected, and the protein concentration was determined using a BCA protein assay kit (Beyotime, China). Protein samples were heated for 10 min at 95 °C with an equal volume of 2X loading buffer.

Fresh retinas were dissected as described previously,[85] and washed twice in phosphate buffered saline (PBS), followed by lysis in 200 μL previously described RIPA buffer supplemented with protease inhibitors. Samples were left on ice for 30 min, followed by boiling at 95 °C with an equal volume of 2X loading buffer for 10 min, then extracted proteins from brains or retinas were separated by 10% sodium dodecyl sulfate polyacrylamide gel electrophoresis (SDS–PAGE) (20 μg protein/lane). Afterward, the proteins were blotted onto polyvinylidene fluoride (PVDF) membranes (Millipore # IPVH00010) using Trans-Blot SD system (Bio-Rad). The membranes with target proteins were blocked with BSA blocking buffer (Sangon Biotech, China # 9048-46-8) at room temperature for 2 h and then incubated with the primary antibody, as indicated in the key resources table, at 4 °C overnight. After washing for three times, the membranes were incubated with the corresponding secondary antibody HRP labeled goat anti mouse IgG or anti rabbit at dilution of (1: 5000) at room temperature for 2 h, followed by washing using TBST (CWBIO, China # CW0043S). Bands were visualized by enhanced chemiluminescence method (ECL) Western blot kits (Advansta, China # K-12045-D10) using FluorChem Q system (Protein simple, USA). The protein band intensity was quantified using the ImageJ program (National Institutes of Health, Bethesda, MD, USA).

Co-immunoprecipitation

For co-immunoprecipitation, cells were lysed in IP lysis buffer (0.5% NP-40; 150 mM NaCl; 20 mM HEPES pH 7.4; 2 mM EDTA, and 1.5 mM MgCl$_2$), supplemented with protease inhibitor cocktail for half an hour, on ice. Cell lysates were incubated with protein A/G beads coated with the indicated antibodies for 4 h at 4°C, and then, the IP products were washed three times with IP lysis buffer. Next, the eluted products were boiled at 95°C for 10 min with an equal volume of 2X loading buffer and the protein extracts were analyzed by SDS–PAGE followed by Western blot analysis.

Quantitative reverse transcription PCR (RT-qPCR)

Total RNAs were extracted from the different mouse organs using TRIzol Reagent (Invitrogen® #15596018) following the manufacturers' instructions. RNase-Free DNase (Promega®, #M6101) was used to eliminate DNA contamination. Reverse transcription was performed using the reverse transcription system (Promega®, #A5001). RT-qPCR was performed using 10 μL aliquots and AceQ qPCR SYBR Green Master Mix (Vazyme® #Q111-03) on a Bio-Rad detection instrument (CFX Connect) according to the manufacturer's specifications. A list of RT-qPCR primers were listed in Table S5.

In vivo- ChIRP

All processes were performed using RNase-free conditions. ChIRP was performed as described,[86] with the following modifications. Young (1 Month) and old (24 Months) mice were perfused with an average of 20 mL

1X PBS, followed by a similar 20 mL perfusion of 1% formaldehyde. The anticipated time from perfusion to completion of dissection was 5 min on average. Each mouse brain was then dissected and homogenized in 1% formaldehyde for 6 min, followed by stripping through a 0.45 μM filter, at 1000 g/5 min/4 °C, followed by 0.125 M glycine quenching for 5 min, and the cell pellet was centrifuged at 1000 g/5 min/4 °C. The cells were washed twice with 1X PBS at 1000 g/5 min/4 °C. Brain cells were separated into multiple tubes, flash frozen in liquid nitrogen, and then kept at −80 °C until further use. Each 0.02 μg cell pellet was lysed in lysis buffer and rotated at 4 °C for 2 h, sonicated for 3–5 min on ice, and then centrifuged at 12.000 rpm/10 min at 4 °C. The lysates were precleared by incubating with 30 μL of washed beads per mL of lysate at 37 °C for 30 min with shaking.

Hybridization with slow rotation took place at 37 °C overnight. The next day, washed Protein A/G beads were added (30 μL) per 1 mL lysate for 2 h at 37 °C, the beads were collected, washed and RNA extraction was performed using a small aliquot of post-ChIRP beads as described.[86] For protein elution, beads were collected on a magnetic stand, re-suspended in biotin elution buffer (12.5 mM biotin (Sigma); 7.5 mM HEPES pH 7.5; 75 mM NaCl; 1.5 mM EDTA; 0.15% SDS, and 0.02% Na-Deoxycholate), mixed at room temperature for 20 min and again at 65 °C for 10 min. The eluent was transferred to a fresh tube, and beads were eluted again. The two eluents were pooled, and residual beads were removed again using the magnetic stand. A 25% total volume of 100% TCA was added to the clean eluent, and after thorough mixing, proteins were precipitated overnight at 4 °C. Then, proteins were pelleted at 16, 000 rpm at 4 °C for 30 min, followed by careful removal of the supernatant and the pellet was then washed once with cold acetone and pelleted again at 16,000 rpm at 4 °C for 5 min. Then the acetone was removed. Pellets were briefly centrifuged again to remove residual acetone and left to air-dry for 1 min at room temperature. Proteins were kept at −80 °C for later mass spectrometry (MS) analysis. See Tables S6 and S7 for the ChIRP probe design, for *Malat1* and *LacZ* respectively.

Mass spectrometry sample preparation

The protein was digested using the Filter Aided Sample Preparation (FASP) process.[87] Briefly, the above eluted ChIRP pull-downed proteins were dissolved in buffer containing 6 M urea, 2 M thiourea, 1X protease and phosphatase inhibitor cocktail (Sigma). Denatured samples were first reduced with 5 mM dithiothreitol (DTT) for 30 min at 56 °C, then alkylated with 20 mM iodoacetamide (IAA) for 30 min at room temperature in dark, followed by incubation with 5 mM DTT for 15 min at room temperature. Subsequently, samples were transferred into 10 kD Microcon filtration devices (Millipore) for filtration at 12, 000 g for 20 min, followed by washing three times with 50 mM NH_4HCO_3. The protein was tryptic digested using an enzyme: protein ratio of 1: 50 for overnight at 37 °C. The resulting peptides were lyophilized on a vaccum freezer (Thermo Scientific) and stored at −80°C until analysis.

Mass spectrometric analysis and database search

Tryptic digested samples were analyzed on an Orbitrap Fusion mass spectrometer (Thermo Fisher Scientific, Rockford, IL, USA) coupled with an Easy-nLC 1000 nanoflow LC system (Thermo Fisher Scientific). Dried peptide samples were reconstituted with Solvent A (0.1% formic acid in water) and loaded onto the traped column (100 μm × 2 cm, homemade; particle size, 3 μm; pore size, 120 Å; SunChrom, USA) and separated on a home-made silica microcolumn (150 μm × 12 cm, particle size, 1.9 μm; pore size, 120 Å; SunChrom, USA). LC separation was performed with a gradient of 5–35% mobile phase B (acetonitrile and 0.1% formic acid) at a flow rate of 600 nL/min for 75 min. The Obitrap Fusion mass spectrometer was conducted in positive mode with an ion spray voltage of 2.3 kV. The precursor scan was set in the range of *m/z* 300–1400 with a resolution of 120, 000 at *m/z* 200 and a maximum injection time of 50 ms with an automated gain control (AGC) target of 5×10^5 in the Orbitrap. For the MS2 scan, the selection of the most intense ions was performed in Quadrupole with the top-speed mode and a window of 1.6 *m/z*, followed by fragmentation with higher-energy collision dissociation with a normalized collision energy of 35%. The MS2 spectra were readout in the ion trap with an AGC target value of 7,000 and a maximum injection time of 35 ms. The dynamic exclusion was set to 18 s.

Label-free quantifications were performed by searching acquired raw files against the mouse UniProt FASTA database (version November 2016) using MaxQuant software (version 1.6.2.0). Trypsin was set as proteolytic enzyme with two missed cleavages allowed. The false discovery rate (FDR) was set to less than 1% for both proteins and peptides. Mass tolerance were set as 20 ppm for the first search peptide tolerance and 4.5 ppm for the main search. Carbamidomethyl cysteine was set as the fixed modification,

and acetylation of the protein N-terminal and oxidation of methionine was set as variable modifications. Proteins identified with two or more unique peptides were reported as true hits. Upon comparing with the *LacZ* control sample, unique hits with an intensity higher than the cut-off value (1×10^6) in old or young brain samples were reported as potential hits for subsequent analysis and validation experiments.

Ubiquitination and Sumoylation assays

N2A cells were transduced with 5 *Malat1* shRNAs and scrambled shRNAs lentiviruses in (6-cm) dish plates. Four hours prior to cell harvesting for the assays, MG132 was added at a concentration of 10 μM. The ubiquitination assay was performed according to a previous report[88] and sumoylation[89] was performed with slight modification. Cells were washed with cold 1X PBS three times. Then, 100 μL of lysis buffer (RIPA buffer, Beyotime, P0013B) was added to the cells, and a cell scrapper was used to collect the cells into 1.5 mL Eppendorf tubes. Immediately, the cells were heated for 10 min at 95°C, followed by 3 strokes of sonication. Then, the cell lysate was diluted with 400 μL of dilution buffer (10 mM Tris–HCl; pH 8.0; 150 mM NaCl; 2 mM EDTA, and 1% Triton) and incubated at 4°C rotator for 30 min. After incubation, lysate was centrifuged at 20,000 *g* for 20 min at 4°C. Supernatant was transferred into Eppendorf tubes containing Protein A/G beads previously coated with P21 antibodies at 4°C rotator for 2 h. After that cell lysates were kept for overnight rotation at 4°C. On the second day beads were collected using magnetic strips and washed three times with wash buffer (10 mM Tris–HCl; pH 8.0; 1 M NaCl; 1 mM EDTA, and 1% NP-40), followed by Western blot analysis, with anti-Ubiquitin as the primary antibody for Ubiquitination assay, and with anti-SUMO2/3 for Sumolation assay.

RNA fluorescence *in situ* hybridization (RNA FISH)

RNA FISH was carried out as described previously.[90] Stellaris® RNA FISH probes were used to visualize the localization of lncRNA *Malat1* according to the manufacturer's instructions. In brief, cells seeded on coverslips were washed with 1X PBS and fixed using 100% ethanol for 10 min at −20°C. Fixed cells were permeabilized overnight in 70% ethanol at 4°C. To hybridize with RNA probes, coverslips were first washed with a wash buffer (50 mM Tris-HCl pH 6.8; 2% SDS; 10% Glycerol; 1% β-mercaptoethanol; 12.5 mM EDTA, and 0.02% Bromophenol blue dissolved in RNase free water) and then incubated upside down with 50 μL of hybridization buffer (1 μg/μL yeast tRNA (Invitrogen #AM7119), 10% formamide (Sigma #75-12-7), 2 mM vanadyl ribonucleoside complex (Sigma #R3380-5 ML), 10% (w/v) dextran sulfate (Sigma #42867), 0.02% Rnase-free BSA (Sangon Biotech, China # 9048-46-8) and 1 μL of RNase inhibitor (Promega #N2615) containing ChIRP probes (see Tables S6 and S7) in a humidified chamber. Incubation took place at 37°C overnight in dark. Coverslips were washed with wash buffer thoroughly the next day followed by incubation with primary mouse anti-biotin (ab201341) antibodies, and Alexa Fluor 488 conjugated Anti-mouse IgG (Proteintech #Alexa Flour 488). The nuclei were counterstained with Hoechst33342 or DAPI. Fluorescent images were visualized using fluorescent inverted microscope (Olympus IX73, Japan), Images were taken using CellSens standard imaging software, followed by deconvolution and maximum protection under the default settings by the operation software.

RNA immunoprecipitation assay

The RNA-immunoprecipitation (RIP) procedure was adapted from a previous publication.[91] Briefly, freshly dissected mouse brains were washed twice in 1X PBS, and homogenized in 1% formaldehyde. Glycine (to final 0.125 M) was added to quench the formaldehyde. Cells were pelleted by centrifugation and washed with 1X PBS. Immunoprecipitation (IP) lysis buffer (20 mM Tris-HCL at pH 8; 0.4 M NaCl; 1 mM EDTA; 0.5% Triton X-100, and 10% glycerol) containing 1 mM PMSF (Roche #1837091001) protease inhibitors (Roche #4906837001) and RNase inhibitor (Promega #N2615) were added to the lysis buffer. After sonication, cell lysate was precleared with washed protein A/G magnetic beads (Thermo#88803 Pierce). 2 μg of the antibody (Lamin A/C Proteintech #10298-1-AP); PHB2 CST #14085); hnRNP C (#SC-32308); KAP1 (Proteintech #15202-1-AP); NPM (Proteintech # 4F12A3) and normal rabbit IgG, (CST #27795)) were separately added to the precleared cell lysate and incubated at 4°C overnight. Washed protein A/G magnetic beads were added and incubated at 4°C for 2 h. A/G beads were washed twice with IP lysis buffer, then re-suspended in 100 μL of IP buffer, 70 μL of which were used for RNA extraction using TRizol LS (Invitrogen #10296-028), DNase I treatment, and 30 μL of which were boiled in 2X Loading buffer for SDS-PAGE. One-step RT-qPCR (Bio-Rad, 1,725,150) was performed with primers listed in Table S5. The results are presented as fold enrichment (normalized to IgG).

Northern blot and densitometry analysis

3′ biotin labeled DNA probes were synthesized by Invitrogen. Total RNAs and RiboRuler High Range RNA Ladder (Thermo Scientific) were resolved on agarose gels containing 1% formaldehyde, and then capillary transferred and UV crosslinked onto a positively charged Nitro Cellulose membrane (Millipore). Hybridization of RNA and biotinylated probes was performed at 42°C overnight; signals were further amplified by HRP-streptavidin and visualized by enhanced chemiluminescence (ChemiScope, CLiNX). Probes for *Malat1* and *LacZ* were listed in (Tables S6 and S7).

mRNA stability assay

mRNA stability assay was carried out as previously described.[92] Briefly, Wild type (WT) and *Malat1*Δ2 NIH3T3 cells were seeded 3×10^5 in 6-well plates. 24 h later the first well was collected as t = 0, and Actinomycin D (ACTD) was added at a concentration of 10 μg/mL. Samples were collected at 2, 4, 8, 12 and 24 h time points following Actinomycin D addition. RNA was extracted using TRIzol Reagent (Invitrogen #15596018), followed by RT-qPCR and data were analyzed as follows: ΔCt = (Average Ct of each time point - Average Ct of t = 0), relative mRNA abundance = $2^{(-\Delta CT)}$. The relative abundance of mRNA at each time point was plotted relative to (t = 0) and the mRNA decay rate was calculated by non-linear regression curve fitting (one-phase decay) using GraphPad Prism.

Retinal histology

Two-month-old wild type (WT), *Malat1*Δ1, and *Malat1*Δ2 mice were anesthetized with 8% chloral hydrate followed by decapitation. Whole eyes were dissected and immersion fixed in 4% paraformaldehyde in 1X PBS overnight at 4°C. The eyes were frozen, cut at 20 μm thickness, and mounted on glass slides. Retinal sections were hydrated in graded ethanol solutions (95%, 75%, 50%) for 30 s each. The retinal sections were then stained with Hematoxylin and Eosin stain as previously described[93] and images were taken using confocal microscopy (Olympus IX73, Japan).

QUANTIFICATION AND STATISTICAL ANALYSIS

Each experiment was repeated two or three times. Statistical differences among groups were analyzed by one-way ANOVA followed by a post-hoc Tukey's test. If two groups were analyzed, the significance was determined by two-tailed t-test (unpaired or paired, as indicated). Statistical significance was established at 0.05 (*$p \leq 0.05$, **$p \leq 0.01$, ***$p \leq 0.001$) using SPSS® software V.21 (Chicago, IL). GraphPad Prism 9.0 was used for statistical illustrations (GraphPad Software, La Jolla, CA, USA).